~~The i~~Improvements in the regional South China Sea Operational Oceanography Forecasting System (SCSOFSv2)

Xueming Zhu[1, 2], Ziqing Zu[2], Shihe Ren[2*], Miaoyin Zhang[2], Yunfei Zhang[2], Hui Wang[3,2*], Ang Li[2]

[1] Southern Marine Science and Engineering Guangdong Laboratory (Zhuhai), Zhuhai, 519000, China

[2] National Marine Environmental Forecasting Center, Key Laboratory of Marine Hazards Forecasting, Ministry of Natural Resources, Beijing, 100081, China

[3]Institute of Marine Science and Technology, Shandong University, Qingdao, Shandong, 266237, China

Correspondence to: Shihe Ren (rensh@nmefc.cn), Hui Wang(wangh@nmefc.cn)

Abstract. The South China Sea Operational Oceanography Forecasting System (SCSOFS), ~~had been~~ constructed and operated by the~~in~~ National Marine Environmental Forecasting Center of China, has been providing ~~to provide~~ daily updated hydrodynamic forecasting in the SCS for the next five~~5~~ days since 2013. This paper presents recent comprehensive updates t~~of~~ the configurations of the physical model and data assimilation scheme in order to improve the ~~SCSOFS~~ forecasting skill of the SCSOFS~~s~~. Th~~e~~is paper highlights three of the most sensitive updates, including the sea surface atmospheric forcing method, the discrete tracer~~s~~ advection ~~discrete~~ scheme, and modification of the data assimilation scheme. Inter-comparison and accuracy assessment among the five versions were performed during the ~~whole~~ entire upgrading process~~es~~ using~~are performed by employing~~ the OceanPredict Inter-comparison and Validation Task Team Class4 metrics. The results indicate that remarkable improvements have been made to the~~achieved in~~ SCSOFSv2 with respect to the original version known as SCSOFSv1. The ~~D~~domain averaged monthly mean root~~-~~-mean~~-~~-square errors of the ~~decrease from 1.21 °C to 0.52 °C for~~ sea surface temperature and~~, from 21.6cm to 8.5cm for~~ sea level anomaly have decreased from 1.21 °C to 0.52 °C and from 21.6 cm to 8.5 cm, respectively.

1. Introduction

The South China Sea (SCS) is located between 2°30′S~~∼~~–23°30′N and 99°10′~~E~~–~~∼~~121°50′E.~~,~~ It is ~~the largest in area and the deepest in depth,~~ a semi-closed marginal sea in the western Pacific and has the largest area and deepest depths. Its area is about 3.5 million km^2, and its maximum depth is about 5300 m in~~at~~ the central region. It is connected~~s~~ to the East China Sea by the Taiwan Strait to the northeast, to the North Pacific Ocean by the Luzon Strait to the east, and to the Java Sea by the Karimata Strait to the south. Numerous islands, irregular and complex coastal boundaries, and drastic changes in bottom topography all ~~together~~ contribute to the extremely~~great~~ complex distribution of the topography in the SCS.

The ~~upper-layer~~ basin-scale ocean circulations in the upper-layer of the SCS are mainly controlled by the East Asian Monsoon (Hellerman and Rosenstein, 1983), result~~show~~ing a cyclonic gyre in winter and an anti-cyclonic gyre in summer (Mao et al., 1999; Chu and Li, 2000). The dynamic multi-scale oceanic circulation ~~dynamical~~ processes in~~of~~ the SCS are affected by various factors, i.e., the Kuroshio intrusion through the Luzon Strait (Nan et al., 2015;Farris and Wimbush, 1996;Liu et al., 2019), the internal waves (Li et al., 2011;Li et al., 2015) and~~or~~ internal solitary waves (Zhang et al., 2018;Zhao and Alford, 2006;Cai et al., 2014) generated in the Luzon Strait and propagated~~ing~~ westward in the northern SCS, the SCS throughflow as a branch from~~of~~ the Pacific Ocean to the Indian Ocean throughflow (Wei et al., 2019;Wang et al., 2011), and energetic mesoscale eddy activities (Zu et al., 2019;Xu et al., 2019;Zhang et al., 2016;Zheng et al., 2017;Hwang and Chen, 2000;Wang et al., 2020). The multi-scale dynamic~~al~~ mechanisms in the SCS are too complex to understand clearly~~ as yet,~~. ~~i~~It has always been a challenge to simulate or reproduce the ocean circulations, as well as~~not~~ to ~~mention~~ forecast the future oceanic status using the~~by~~ Operational Oceanography Forecasting System (OOFS).

Within the coordination and leadership of the Global Ocean Data Assimilation Experiment OceanView (GOV, https://www.godae-oceanview.org; Tonani et al., 2015;Dombrowsky et al., 2009), in the last~~recent~~ decade or two, several regional OOFSs have been developed and operated based on the state-of-the-art community numerical ocean models for~~in~~ different regions of the ocean. Tonani et al. (2015)

reported~~summarized~~ that a total of~~there were~~ 19 regional systems were running operationally ~~in total~~ untill 2015.

For instance, the Canadian Operational Network of Coupled Environmental Prediction Systems from Canada was built based on the Nucleus for European Modelling of the Ocean (NEMO) 3.1, and its~~whose~~ domain covered the Arctic and North Atlantic oceans with a 1/12° horizontal resolution.~~;~~ ~~t~~The Real-Time Ocean Forecast System of the~~from~~ US National Oceanic and Atmospheric Administration National Cent~~e~~res for Environmental Prediction (NCEP) was designed based on the HYbrid Coordinate Ocean Model and was implemented in the North Atlantic on a curvilinear coordinate system, with a~~the~~ horizontal resolution ranging from 4 km to 18 km.~~ in horizontal;~~ The Meteorological Research Institute (MRI) of the Japan Meteorological Agency developed the Multivariate Ocean Variational Estimation System/MRI Community Ocean Model (MOVE/MRI.COM) coastal monitoring and forecasting system based on the MRI.COM (Tsujino et al., 2006). This~~e~~ model consists of a fine-resolution (2 km) coastal model around Japan and an eddy-resolving (10 km) Western North Pacific model with one-way nesting.~~;~~ ~~t~~The Chinese Global operational Oceanography Forecasting System was developed and operated based on the Regional Ocean Modelling System (ROMS, Shchepetkin and McWilliams, 2005) and NEMO by the National Marine Environmental Forecasting Center, covering six~~6~~ subdomains from global to polar regions, Indian Ocean, Northwest Pacific, Yellow Sea and East China Sea (Kourafalou et al., 2015), and S~~outh ~~C~~hina ~~S~~ea~~ (Zhu et al., 2016), with ~~their ~~horizontal resolutions ranging from 1/12° to 1/30°. It ~~is~~should be noted~~ worth noting~~ that there are considerable differences among th~~o~~ese systems in many aspects, such as the model codes, area coverage, horizontal and~~/~~ vertical resolutions, and data assimilation schemes, which are based on~~and so on, according to~~ the user needs and~~or~~ regional ocean characteristics. In order to better satisfy the end users' needs, these OOFSs ha~~s~~ve been upgraded~~ing~~ and improved~~ing~~ constantly since they began operation. In general, most improvements to the~~of~~ OOFSs we~~a~~re implemented by increasing the horizontal or vertical grid resolution, changing the data assimilation schemes ~~in~~to a more sophisticated level, assimilating more diverse sources of observation data, and by benefiting from the growth of high-performance computing power and global or regional observation networks. Initially, the MOVE/MRI.COM was developed based on a three-dimensional variational analysis scheme and was implemented in 2008 (Usui et al., 2006)., tThen, it was updated to athe four-dimensional variational analysis scheme to provide better representation of mesoscale processes (Usui et al., 2017). The Mercator Ocean International global monitoring and forecasting system had been routinely operated in real time with an intermediate-resolution ofat 1/4° and 50 vertical levels since early 2001. An uUpgrading byof increasing the horizontal resolution was implemented in December 2010, to consisting of a 1/12° nested model over the Atlantic and Mediterranean. Real time daily services with a global 1/12° high-resolution eddy-resolving analysis and forecasting were delivered by an updated system, since 19 October, 2016. Moreover, Mercator Ocean International also continues to implement regularly updates by increasing the system's complexity, such as expanding the geographical coverage, improving the models, and assimilating schemes, and have developinged several versions for the various milestones of the MyOcean project and the Copernicus Marine Environment Monitoring Service (Lellouche et al., 2013, 2018).

As mentioned in the literature of Zhu et al. (2016), the regional SCS Operational Oceanography Forecasting System (SCSOFS, here after named it as SCSOFSv1) has been developed and routinely operated in real time since the beginning of 2013. It has continued to be upgraded by modifying the model settings in many aspects, such as the mesh distributions, surface atmospheric field forcing, and open boundary inputs, and so on, andby improving the data assimilation scheme according to the results of comparisongs and validationsg fromconducted by Zhu et al. (2016), in order to provide better services. The primary purpose of this studypaper wa iss to introduceing the updates applied to SCSOFS and to determine which update had the great, but only show the highestest impact on the system. The other results offrom routine system updates andor improvements werewill not determinedbe illustrated or analyseddiscussed in detail.

This paper is organized as follows. A detailed description of some general/basic updates applied to the SCSOFS iswill be provided in Section 2. Some highlights and sensitive updates and their impacts ton the performance of the system are describedshown in Section 3. The Rresults of the inter-comparison and assessment ofor the different SCSOFS versions during the upgrading processes based on the 'Class 4 metrics~~'~~ verification framework (Hernandez et al., 2009) are presented~~will be shown~~ in Section 4. Section 5 contains a summary of the scientific improvements and future plans for the next step.

2. Physical model description, updates, and input datasets

This section describes several~~some~~ general updates applied to the SCSOFSv1 in the last few~~recent couple~~ years. The newly updated system is referred~~named~~ to~~as~~ SCSOFSv2 in this paper~~here after~~. In order to isolate the contributions of each modification, different simulations were performed for the respective updates. However, some of the updates were~~have been~~ implemented directly according to model experiences or theoreticaly~~y~~ knowledge~~s~~, without standalone evaluation. The performances of~~from~~ a few integrated updates will be shown in Section 4 in~~for~~ the different upgrading stages.

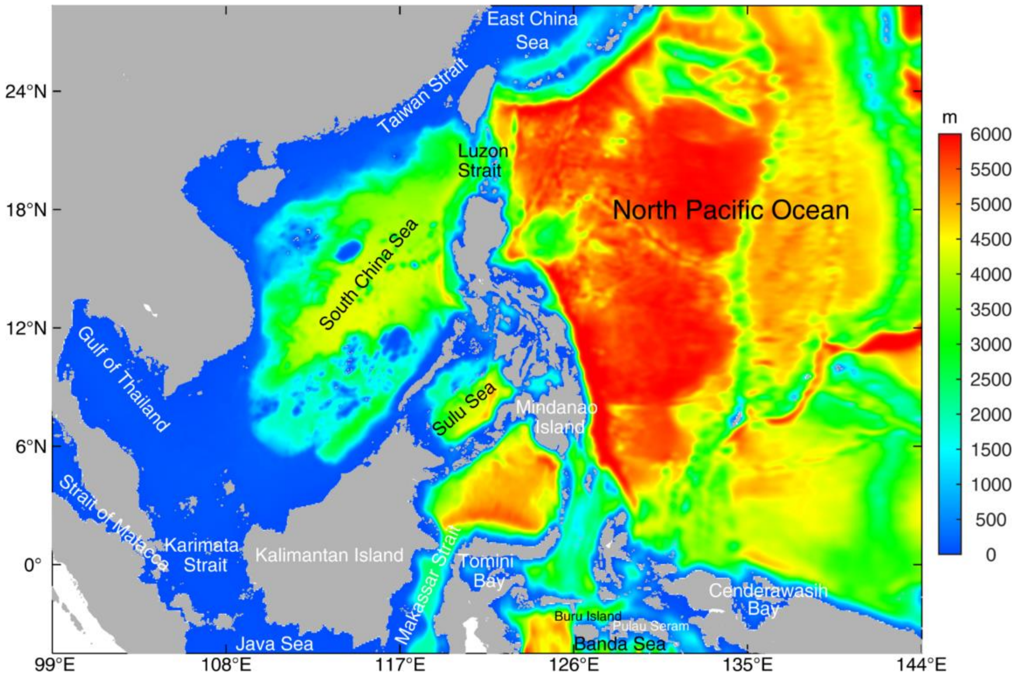

Figure 1: The model domain and bathymetry of SCSOFSv2

The SCSOFSv2 is still built based on ROMS, whichle~~le whose version~~ has been updated from v3.5 (svn trunk revision 648 in 2013) to v3.7 (svn trunk revision 874 in 2017). In addition to a~~ROMS v3.7 incorporates some changes for the model settings, which facilitating the operational running especially, besides of the~~ major overhaul of the nonlinear, tangent linear, representor, multiple-grid nesting, and adjoint numerical kernels, ROMS v3.7 incorporates several changes to the model settings, which facilitate the operational running.

Firstly, we redistributed the land-sea grid mask layout to enable the systems mesh land boundary to fit the actual coastline better (Fig.1). Based on aBy comparisiong with the Fig. 1 infrom Zhu et al. (2016), a few areas haved been changed from land to sea or vis versainverse, e.g., along the coast of China mainland, the Vietnam and the Gulf of Thailand, and around the coasts of the Kalimantan Island and the Mindanao Island. In addition, the Strait of Malacca had been opened to connect with the Karimata Strait, and the western lateral boundary was treated as an open boundary across the Strait of Malacca along 99°E, instead of as a closed boundary as in SCSOFSv1.; aAlong the south lateral open boundary, the Java Sea was connected to the Makassar Strait toin the southeast of the Kalimantan Island, the Banda Sea was connected across the southern part of Buru Island and Pulau Seram,; and includingvolved the Tomini Bay and the Cenderawasih Bay. It is obvious that the changes in the land-sea masks changing can generated significant effects on the sea water volume of sea water transportation in the model domain, and thus, it would contributes to the better simulation of the ocean circulations.

The bathymetry ETOPO1 dataset used in SCSOFSv1, which has a 1 arc-minute grid resolution from the U.S. National Geophysical Data Center, was is replaced by the General Bathymetric Chart of the Oceans (GEBCO_2014 Grid) global continuous terrain model for ocean and land, which has ais with 30 arc-second spatial resolution in SCSOFSv2, from ETOPO1 data set in SCSOFSv1, which is with 1 arc-minute grid resolution from U.S. National Geophysical Data Center. It wais also merged with the measured topographic data in the coastal areas along China mainland, and was adjusted with the tidal range. Then, it wais smoothed by applying a selective filter 8eight times to reduce the isolated seamounts on the deep ocean, so that the “slope parameter” $r=\Delta h/2h$ is lower than thea maximum value r_0=0.2 for each grid (Beckmann and Haidvogel, 1993; Marchesiello et al., 2009), in order to supress the computational errors of the pressure-gradient (Shchepetkin and McWilliams, 2003). Then, the two grid stiffness ratios parameters, i.e., the slope parameter (r) and the Haney number, were changed from 0.22 and 9.78 in SCSOFSv1 to 0.17 and 13.80 in SCSOFSv2, respectively. The maximum depth was isstill set to be 6000 m still, but the minimum depth was changed from 10 m in SCSOFSv1 to 5 m in SCSOFSv2 (Wang, 1996). The final smoothed bathymetry is shown in Fig.1.

For the vertical terrain-following coordinate, it hwas been increased from 36 s-coordinate layers in SCSOFSv1 to 50 layers in SCSOFSv2. The transformation equation ofrom the original formulation wais also changed to an improved solution (Shchepetkin and McWilliams, 2005). The original vertical stretching function (Song and Haidvogel, 1994) wais replaced with an improved double stretching function (Shchepetkin and McWilliams, 2005), to make it preserve a sufficient resolution in the upper 300 m in order to resolve the thermocline well. In this case, the thinnest layer was changeds from 0.16 m in SCSOFSv1 to 0.09 m in SCSOFSv2 near the surface.

The new initial temperature and salinity fields in SCSOFSv2 weare extracted from the Generalized Digital Environmental Model version 3.0 (GDEMv3, Carnes, 2009) global climatology monthly mean in January, which replacedto substitute the version 2.2.4 of the Simple Ocean Data Assimilation (SODA, Carton and Giese, 2008) datasets. All four lateral boundaries are open, and thewhose temperature, salinity, velocity, and elevation are obtained viaprescribed by spatial interpolation offrom the new SODA 3.3.1 datasets for the running 2005–-2015 and SODA 3.3.2 datasets for the running 2016–-2018 datasets (Carton et al., 2018), instead of the original SODA 2.2.4. In the current versionthis present, we use the SODA 3.3.1/2 monthly mean ocean state variables are used, which are mapped onto the regular 1/2°×1/2° Mercator horizontal grid from the original approximately 1/4°×1/4° displaced pole non-Mercator horizontal grid at 50 -z vertical levels.

For the surface atmospheric forcing, we replaced the dataset from the NCEP Reanalysis 2 provided by the NOAA/OAR/ESRL PSL, Boulder, Colorado, USA, which is accessible from their website at https://psl.noaa.gov/ (Kanamitsu et al., 2002), with the six6-hourly Climate Forecast System Reanalysis (CFSR, Saha et al., 2010) for 2005–-2011 and the Climate Forecast System version 2 (CFSv2, Saha et al., 2014) for 2011–-2018. Both are archived at the National Centere for Atmospheric Research, Computational and Information Systems Laboratory, Boulder, Colorado., Itswith a 0.2°–-0.3° horizontal grid is significantly higher horizontal grid than the 2.5°×2.5° resolution of thefor NCEP Reanalysis 2.

The net surface heat flux correction ~~is~~ still follows~~ing~~ Barnier et al.~~ (1995)~~'s (1995) method in SCSOFSv2, but the parameter dQ/dSST, i.e., the~~ of~~ kinematic surface net heat flux sensitivity to sea surface temperature (SST), is calculated using the SST, sea surface atmospheric temperature, atmospheric density, wind speed, and sea level specific humidity, instead of setting a constant number of −~~-~~30 W m^{2} K^{-1} for the entire~~whole~~ domain as in SCSOFSv1. Therefore, the parameter dQ/dSST varies temporally and spatially. In addition~~Meanwhile~~, ~~we use~~ the infrared Advanced Very High Resolution Radiometer (AVHRR) satellite data are used in SCSOFSv2, which is an analysis constructed by combining observations from different platforms on a regular grid via optimum interpolation and is provided by the National Cent~~e~~res for Environmental Information, instead of ~~using~~ the merged satellite's infrared~~ sensors~~ and microwave sensor, and the *in-situ* (buoy and ship) ~~data~~ global daily SST (MGDSST) data obtained from the Office of Marine Prediction of the Japan Meteorological Agency used in the SCSOFSv1.

The North Equatorial Current (NEC) is an interior Sverdrup steady current in the subtropical North Pacific and is located at~~ about~~ 10–~~°N-~~20°N.~~,~~ It~~and~~ usually bifurcates into two branches after encountering the western boundary along the Philippine coast to~~in~~ the west of 130°E (Qiu and Chen, 2010). However, the NEC is separated into two branches in the SCSOFSv1 due to~~affected by~~ the model's eastern lateral boundary setting~~,~~. ~~i~~Its main branch is located at~~ about~~ 9.5~~°N~~–~~-~~13°N, and the other branch is located at 14.5–~~°N-~~17°N (Fig. 2a), which is clearly not in line with the actual locations~~fact~~. The cause of the~~for~~ above result is that ~~the~~ Guam ~~Island~~ (~~shown in~~ red circle in Fig. 2, located at about 13°26′N, 144°43′E) is included in SCSOFSv1, and its~~whose~~ location is too close to the eastern lateral boundary. There is a sudden change in~~ of~~ the bathymetry from over 3500 m to below 500 m, serving as a large~~big~~ blockade to the NEC that once flowed~~ing~~ into the model domain from the eastern lateral boundary. To resolve this problem, in SCSOFSv2, the eastern lateral boundary w~~h~~as ~~been~~ moved westward from 145°E to 144°E to narrow the model domain and exclude ~~the~~ Guam~~ Island in SCSOFSv2~~. It wa~~i~~s found that in SCSOFSv2, the simulated NEC remains as ~~keeps the form of~~ one main current until 130°E ~~,~~and then bifurcates into the southward-flowing Mindanao Current and the northward-flowing Kuroshio~~ in SCSOFSv2~~ (Fig. 2b). ~~Also~~In addition, it ~~i~~has been shown that the Kuroshio current of eastern Philippine Island and the ocean circulations in theof north-eastern SCS greow stronger whenile the island of Guam wasgot removed. ThisIt indicates that the location of the lateral open boundary is very important to the results of the model's simulation, and the results areit would be better when it isif being set to far enough away from the island, especially forwhile the islands located in the major ocean circulations.

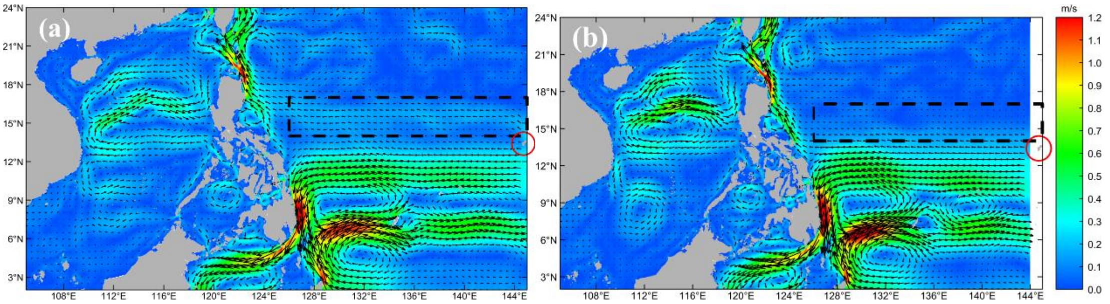

Figure 2: The multi-year monthly mean sea surface currents (the colour shading indicates theed for current speed (m s^{-1}), and the arrows denote thefor current direction) with vertical averagesd of >above 100 m in May. The left panel (a) is from SCSOFSv1, with the model domain including the Guam Island, the right panel (b) is from SCSOFSv2, with the eastern lateral boundary moveding 1 degree westward.

For the advection schemes of the momentum, third-order upstream and fourth-order centered schemes weare used in both the horizontal and vertical directions. A Hharmonic mixing scheme wais used for both the viscosity for momentum and the diffusion for tracers in the horizontal. The Mellor-Yamada Level-2.5 vertical turbulent mixing closure scheme wais used for both the momentum and tracers. In SCSOFSv2, theyAll of them in SCSOFSv2 are all set theto be same as in SCSOFSv1. Table 1 summarizes the main differencest characteristics between SCSOFSv1 and SCSOFSv2 after upgrading.

Table 1 The main differencest characteristics between SCSOFSv1 and SCSOFSv2

System settings		SCSOFSv1	SCSOFSv2
ROMS version		V3.5	V3.7
Bathymetry		ETOPO1	GEBCO_2014
Initial conditions		SODA2.2.4	GDEMv3
Open boundary cConditions		SODA 2.2.4 climatological monthly mean	SODA3.3.1 and SODA 3.3.2 monthly mean
Sea surface atmospheric forcing	Data	NCEP Reanalysis 2	CFSR
	Method	Directly fluxes forcing	COARE3.0 Bulk Formula
The parameter of dQ/dSST		Constant (-–60)	Calculated with spatiotemporal variations
Observed SST data used for net surface heat flux correction		MGDSST	AVHRR
The pPosition of eastern lateral boundary		145°E	144°E
Vertical layers		36	50

Horizontal advection scheme of tracers	Third-order upstream	Fourth-order Akima
Vertical advection scheme of tracers	Fourth-order centered	Fourth-order Akima
Horizontal mixing surface	Constant density	Geopotential surfaces
Assimilated observation data	SLA	SLA, AVHRR, Argo profiles

The SCSOFSv2 is run using~~with~~ a 5 s time step for the external mode, and a 150 s time step for the internal mode under all of the new configurations described~~mentioned~~ above and those that will~~to~~ be introduced in Section 3. The reason for the modification~~ying~~ of the time step is related to the change in~~of~~ the discrete schemes, which will be illustrated further in Section 3. First, a~~A~~ 26-~~-~~year~~s~~ climatology run is conducted for spinning-up~~ at first~~, ~~and~~ followed by a hindcast run from 2005 to 2018 (Wang et al., 2012). The daily mean of the model results is archived and used for the subsequent evaluation.

3. Highlights, ~~and~~ sensitive updates, and their impacts

Most of the bias and~~or~~ errors in the operational systems are mainly induced by several some major recurring problems, for example, external forcing, the intrinsic deficiencies of the numerical model (e.g., discrete schemes and sub-grid scale~~,~~ parameterization schemes~~ for sub-grid scale~~), initial errors, and the assimilation schemes. In this section, we elaborate upon the solutions to such problems that are applied in SCSOFSv2, which were~~has~~ not discussed~~been mentioned~~ in Section 2. All of these solutions~~them~~ have significantly improved the model skill~~s~~ of the SCSOFS from different aspects, such as the SST, the three-dimensional temperature and salinity structures, and the comprehensive simulation~~g~~ skill, especially for the meso-scale processes.

3.1 Sea surface atmospheric forcing

The air-~~-~~sea interactions are~~is~~ one of the most essential physical processes that affect the vertical mixing and thermal structure of the upper~~-~~ ocean. The air-~~-~~sea fluxes mainly include the momentum flux, fresh water flux, and heat flux. The SST is an important indicator of the ocean circulation, ocean front, upwelling, and sea water mixing, and its~~whose~~ variations mainly depend~~ing~~ on the air-~~-~~sea interactions~~,~~ and the ocean's thermal and dynamic~~al~~ factors (Bao et al., 2002). Thus, for the OOFS and ocean numerical modelling, the SST simulation and forecasting accuracy of SST is anone important metric forto evaluatinge the modelling and forecasting performance.

The accurate input of the sea surface atmospheric forcing plays a key role to excel in the performance of the model simulation of the SST. The ROMS provides two methods tof introducinge the sea surface atmospheric forcing: one is directly forcing the ocean model by providing momentum fluxes (wind stress), net fresh water fluxes, net heat fluxes and shortwave radiation fluxes from the atmospheric datasets; the other is employing the COARE3.0 bulk algorithm (Fairall et al., 2003) to calculate the air-–sea momentum, fresh–water, and heat turbulent fluxes using the set of atmospheric variables from the atmospheric datasets, including the wind speed at 10 m above the sea surface, the mean sea level air pressure, the air temperature at 2 m above the sea surface, the air relative humidity at 2 m above the sea surface, the downward longwave radiation flux, the precipitation rate, and the shortwave radiation fluxes (Large and Yeager, 2009). The calculations ofor the air-–sea fluxes, sensible heat flux, latent heat flux, and longwave radiation can be referenced to Li et al. (2021). Since the SST useding in the calculation of thoese three air-–sea fluxes is extracted from the ocean model, anthe increase in the of SST induces their variations in these fluxesas a result, which then leads to increaseding loss of ocean heat, and inhibitsing further increases in the of SST;, and vice versa. Thus,It means that an effective negative feedback mechanism canould form between the SST and the SST-related heat fluxes. In this case, it is much easier to maintain the simulated SST at a reasonable level. The first method is employed in SCSOFSv1, and the second method, i.e., the bulk algorithm, is employed in SCSOFSv2.

In order to evaluate the performances of the different sea surface atmospheric forcing methods, we conducted a special experiment by changing the method based on SCSOFSv1, which is referred to as BulkFormula here named the experiment in this paperas BulkFormula. In this experiment, we used the merged satellite SST analysis with a multi-scale optimal interpolation, called the Operational SST and Sea Ice Analysis (OSTIA) system, whiceth globally coverage on a daily basis atnd a horizontal grid resolution of 1/20° (~6 km), which is and produced by the Met Office (Donlon et al., 2012), to verify the results of the SCSOFS.

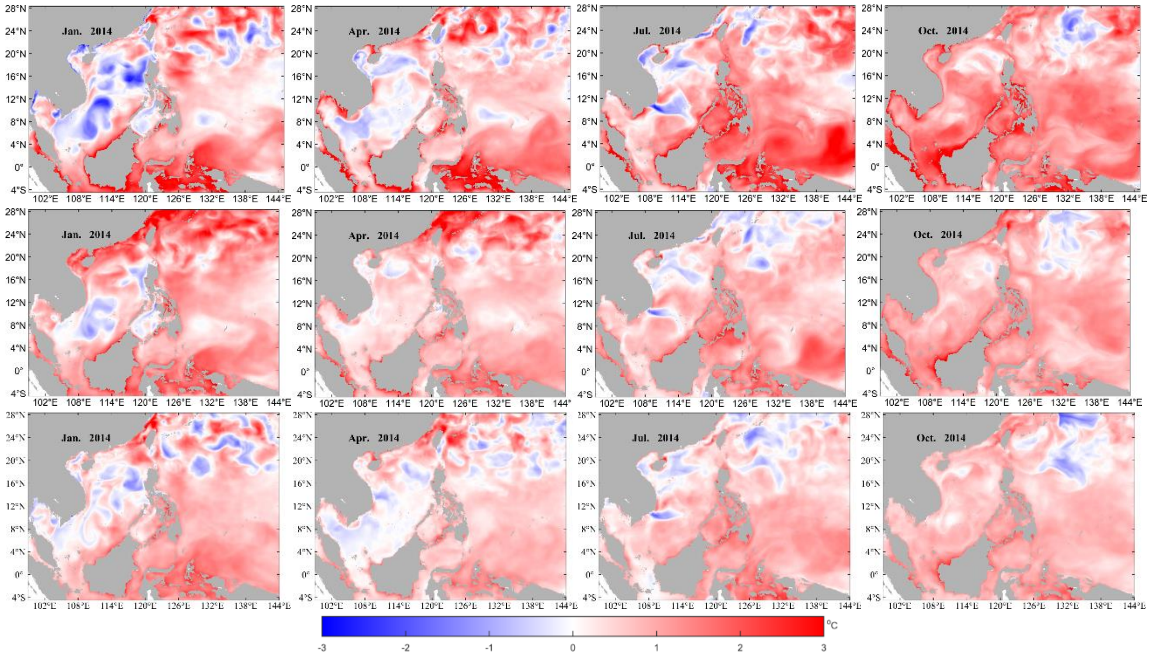

Figure 3: The monthly mean SST differences in January, April, July, and October~~,~~ of 2014: SCSOFSv1 minus OSTIA (upper panels), BulkFormula minus OSTIA (middle panels), SCSOFSv2 minus OSTIA (lower panels)

Figure 3 shows the distributions of the monthly mean SST differences in January, April, July, and October of~~,~~ 2014, which represent~~to stand for~~ ~~W~~winter, ~~S~~spring, s~~S~~ummer, and ~~A~~autumn, respectively. The SST differences we~~a~~re calculated using~~with~~ SCSOFSv1, BulkFormula, and SCSOFSv2 minus~~subtracts~~ the OSTIA~~, respectively~~. It ~~i~~was found that the simulated SST we~~a~~re higher than the OSTIA in all three sets of results. The difference from SCSOFSv1 is significantly~~pronouncedly~~ higher than the differences from the BulkFormula and SCSOFSv2. The maximum differences mainly occur near the coast (~~Fig.3~~ upper panels in Fig.3), especially for a few bays embedded in~~to~~ the mainland, which are~~is~~ nearly impossible to resolve well using~~with~~ 2–~~-~~3 horizontal grids with ~~a~~t 1/30° resolution and with~~in~~ very shallow water depth in SCSOFSv1. This is because the sea surface atmospheric forcing data are~~is~~ not accurate enough near the coast, and they provide an abnormally high~~er~~ amount of heat to the ocean, resulting in~~causing the~~ continuous~~ly~~ heating of the coastal water. Thus, the simulated SST is beyond the normal level in SCSOFSv1. This phenomenon can be significantly alleviated ~~significantly~~ by introducing the effective negative feedback mechanism between the model's SST and the air-sea heat flux using~~by employing~~ the COARE 3.0 bulk algorithm, which is employed in both the BulkFormula and SCSOFSv2 (Fig.3 middle and lower panels).

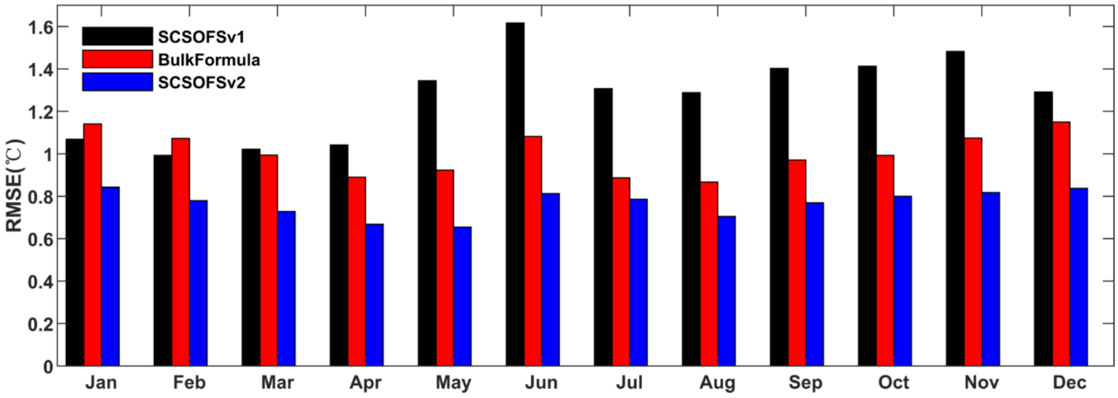

Figure 4: Domain averaged monthly mean SST RMSE comparison of the~~among~~ SCSOFSv1 (black), BulkFormula (red), and SCSOFSv2 (blue) with the~~and~~ OSTIA SST in January, April, July, and October of~~,~~ 2014

Figure 4 shows the bars of the domain averaged ~~R~~root-~~M~~mean-s~~S~~quare ~~E~~error (RMSE) of the monthly mean SST differences between~~of~~ SCSOFSv1, BulkFormula, and SCSOFSv2 with respect to the OSTIA datasets for~~in~~ each month in~~of~~ 2014. It wa~~i~~s found that the domain averaged RMSE of the monthly mean SST differences for~~om~~ SCSOFSv1 is ~~about~~ 0.99 °C–~~-~~1.62 °C, and the annual mean value is about 1.27 °C. The highest (1.62 °C) is in June, and the lowest (0.99 °C) is in February. The ~~M~~monthly mean RMSE for the BulkFormula run is ~~about~~ 0.87 °C–~~-~~1.15 °C, and the annual mean value is about 1.00℃.~~,~~ ~~t~~The maximum value (1.15 °C) is in January and December, and the minimum value (0.87 °C) is in August. The performance of the model's skill for the annual mean SST RMSE is~~can be~~ improved by about 21% ~~only~~ by changing the ~~method of~~ sea surface atmospheric forcing method from direct~~ly~~ forcing to the COARE 3.0 bulk algorithm due to the effective negative feedback mechanism.

However, the domain averaged RMSE of the monthly mean SST differences for~~om~~ the SCSOFSv1 is lower than that for~~om~~ the BulkFormula in January and February, especially in the shallow region around ~~the~~ Taiwan~~ Island~~. This~~It~~ indicates that the COARE 3.0 bulk algorithm is not necessarily a panacea, even with an effective negative feedback mechanism. This may be dependent on the surface forcing~~ field~~ data ~~dependent~~, and the use of an accurate dataset for~~f~~ the sea surface atmospheric forcing is more important~~effective~~ than the selection of the forcing method~~ology selection~~ (Li et al., 2019). It also may suffer from the complicated air–~~-~~sea interactions and tidal mixing missing~~ed~~ in the model.

3.2 Discrete t~~T~~racers advection term ~~discrete~~ schemes

Spurious diapycnal mixing is one of the traditional errors in state-of-the-art atmospheric and oceanic models, especially for regional~~the~~ terrain~~-~~-following coordinate ~~regional~~ models, including both the continental slope and deep ocean (Marchesiello et al., 2009; Naughten et al., 2017; Barnier et al., 1998). Marchesiello et al. (2009) identified the problem as~~of~~ the erosion of the salinity from the southwest Pacific model with steep reef slopes and distinct intermediate water masses based on the ROMS. They found that the ROMS cannot preserve the large-scale water masses while using the third-order upstream advection scheme during the spin-up phase of the model, and they proposed a rotated split upstream third-order scheme to decrease the dispersion and diffusion by splitting the diffusion from the advection. They implemented the rotated split upstream third-order scheme by employing a rotated biharmonic diffusion scheme with flow-dependent hyper diffusivity satisfying the Peclet constraint.

For SCSOFSv1, a third-order upstream horizontal advection scheme, a fourth-order cent~~e~~red vertical advection scheme, and a~~the~~ scheme of

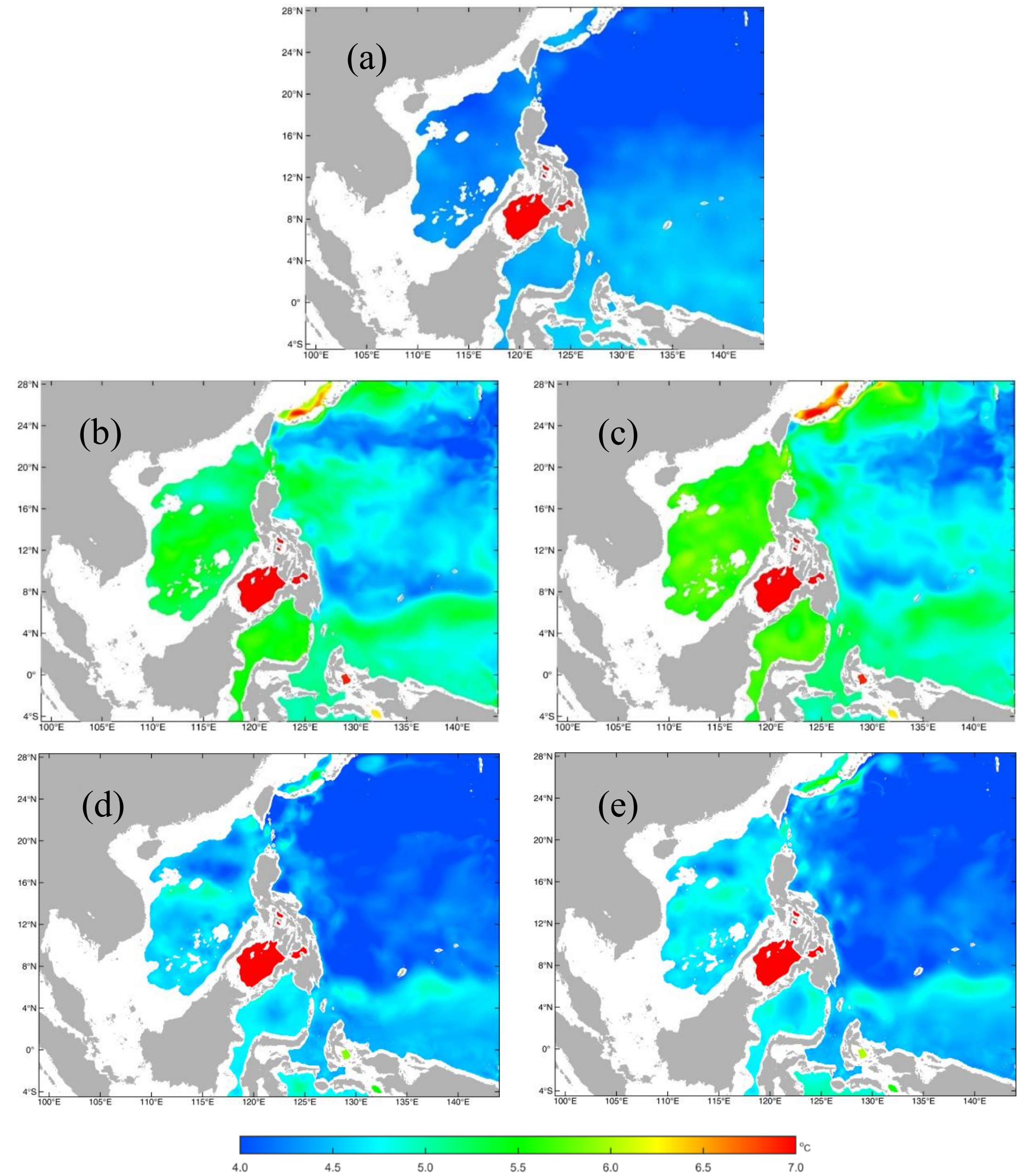

Figure 5: The distributions of the monthly mean temperature in~~at~~ the 1000 m layer in January from the (a) GDEMv3 climatology ~~(a)~~, (b) the fifth ~~(b)~~ and (c) the 11~~eleven~~th ~~(c)~~ model year ~~by~~ using the scheme combination of the UCI based on SCSOFSv1 for other model settings, (d) the fifth ~~(d)~~ and (e) the 11~~eleven~~th ~~(e)~~ model year ~~by~~ using the scheme combination of the AAG based on SCSOFSv2 for other model settings.

horizontal mixing on epi-neutral (constant density) surfaces for tracers we~~a~~re selected (Shchepetkin and McWilliams, 2005). We ~~have~~ encountered same problem with Marchesiello et al.'s (2009) method regarding the~~for~~ temperature (Fig.5b and 5c) and salinity (Fig.6b and 6c) in the deep layer. Figure 5 and 6 show the distributions of the monthly mean temperature and salinity in the~~at~~ 1000 m layer in January from the GDEMv3 climatological initial fields, as well asand the simulated results from the fifth and the 11eleventh model years by using 1) the scheme combinations of the third-order upstream horizontal advection, fourth-order centered vertical advection, and horizontal mixing on epi-neutral surfaces (hereafter referred to as UCI) and 2) the combination of the fourth-order Akima scheme (Shchepetkin and McWilliams, 2005) for both the horizontal and vertical advection terms and the scheme of horizontal mixing along Geopotential surfaces (constant Z) for tracers (hereafter referred to as AAG), respectively., Theand other settings are identical to those ofwith SCSOFSv2. Figure 7 shows the comparisons of the time series of the domain averaged monthly mean temperature and the salinity in theat 1000 m layer simulated using the scheme combinations of the UCI in SCSOFSv1 and the AAG in SCSOFSv2, respectively. In order to lowersave computation costs, we only raun the model with the scheme combination of the UCI for over 16 years untill it reachesd a stable stateus.

The fourth-order Akima scheme is a little different from the fourth-order centered scheme because it replacesby replacing the simple mid-point average with harmonic averaging in the calculation of the curvature term. Since the time stepping is done independently of the from spatial discretization in the ROMS, the Akima scheme has therepresents its advantage of reducing the spurious oscillations, which arises fromwith the non-smoothed advected fields, with respect to the fourth-order centered scheme (Shchepetkin and McWilliams, 2003, 2005).

During the spin-up phase of the model from the initial conditions derived from GDEMv3, the temperature at 1000 m increases from the3.0-12.0℃ by initial settings of 3.0 ℃-12.0 ℃ (Fig.5a) to 3.0 ℃-17.2℃ (Fig.5b), and the domain averaged monthly mean value quickly increases from 4.4 ℃ to 5.1 ℃ (Fig.7a) in

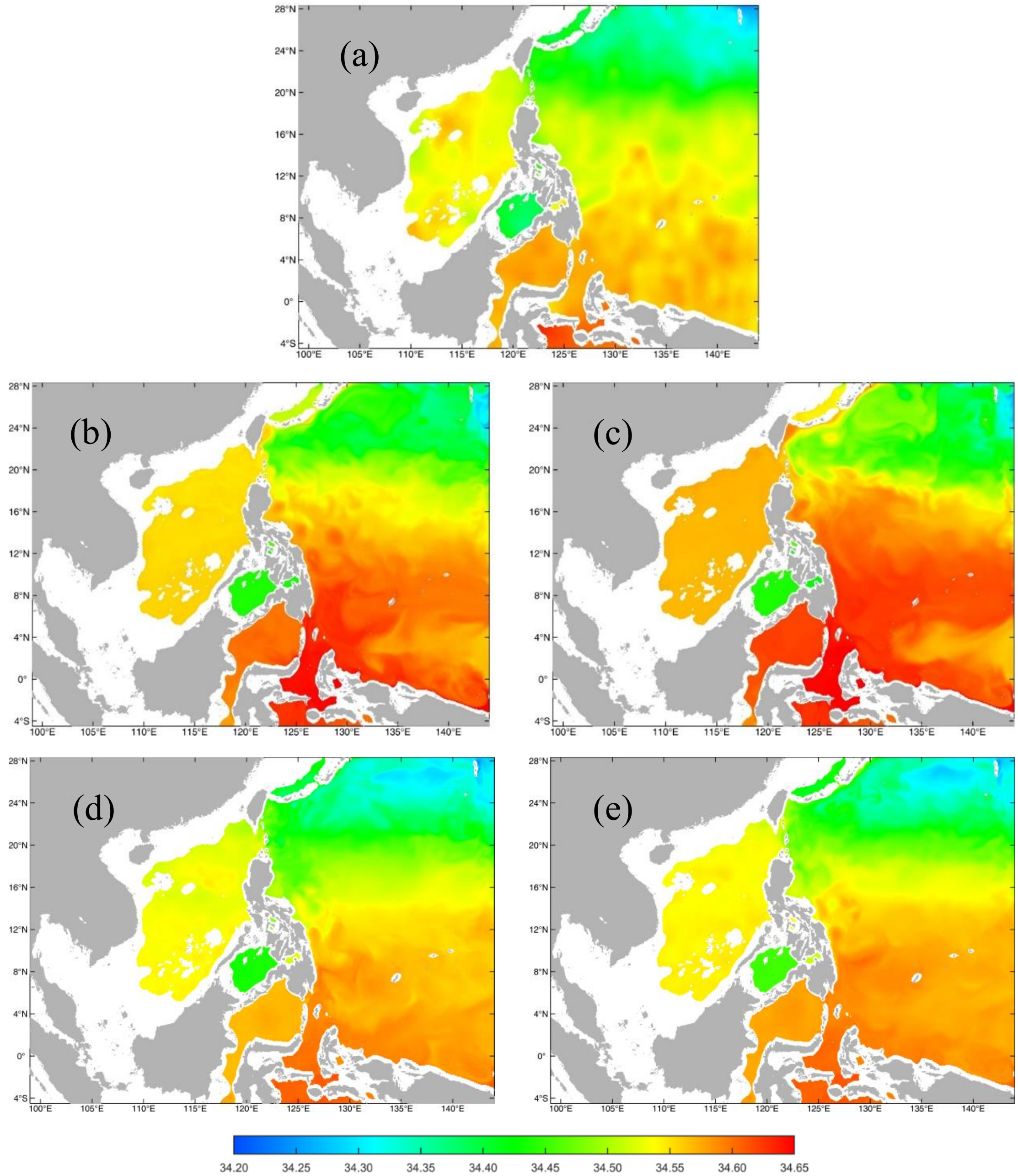

Figure 6: The same as Fig. 5, but for salinity.

January of the fifth model year;. tThe salinity at 1000 m increases from the initial settings of 34.26 – 34.62 by initial settings (Fig.6a) to 34.27 – 34.68 (Fig.6b), and the domain averaged monthly mean value increases rapidly from 34.50 to 34.54 (Fig.7b) in January of the fifth model year – too. In particularEspecially, the increase ing the of domain averaged monthly mean value is almost linearly for both the temperature and salinity in the first 50 months, indicating a fast rate of increase speed and strong spurious diapycnal mixing (Fig.7). Theose values are even higher in January inof the 11eleventh model year, the ranges (minimum and maximum values) reach ~~to~~ 3.0 °C–17.3 °C ~~for temperature (Fig.5c)~~ and 34.26-34.73 for temperature (Fig.5c)~~for~~ and salinity (Fig.6c), respecitvely. The domain averaged values are 5.3 °C for temperature and 34.56 for salinity (Fig. 7)~~, respectively~~. The areas with increasing temperature and salinity are mainly located on the~~at~~ steep slopes and nearby regions, e.g., the central basin of the SCS, the Sulawesi Sea, and the equatorial Pacific Ocean.

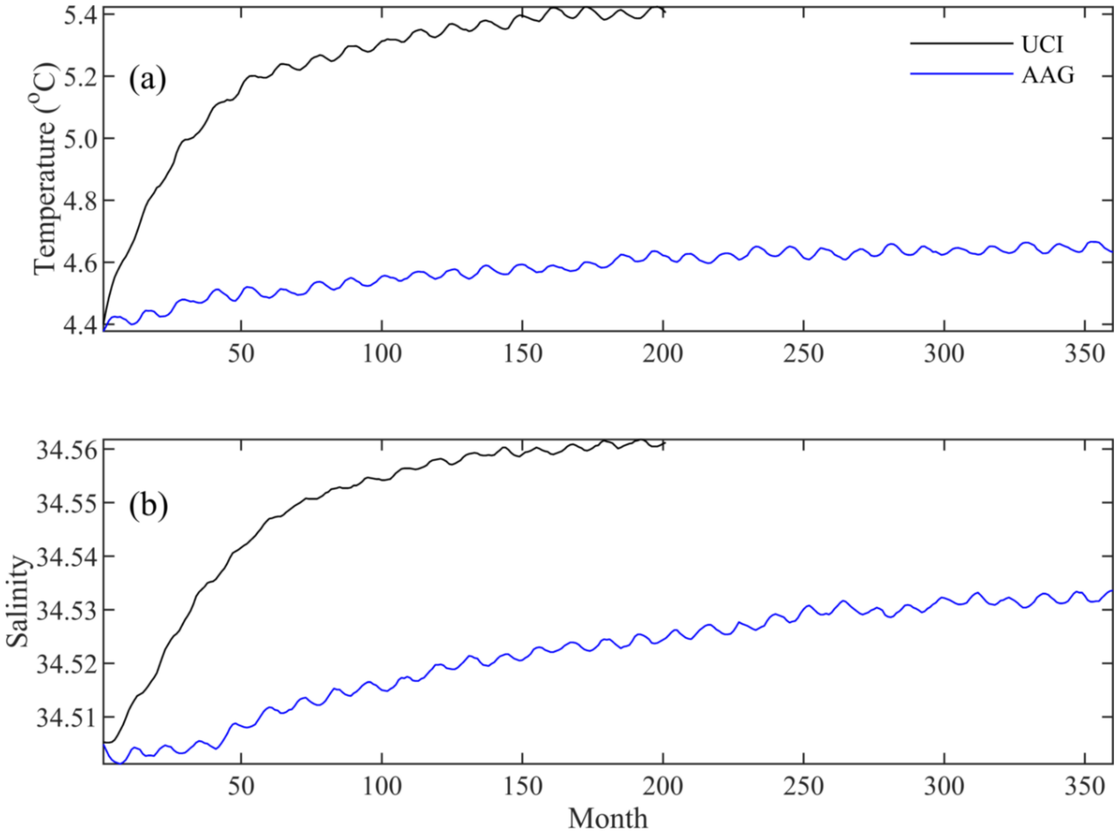

Figure 7: The timeseries of the domain averaged monthly mean (a) temperature ~~(a)~~ and (b) salinity in the~~(b)~~ ~~at~~ 1000 m layer simulated ~~by~~ using the scheme combinations of UCI (black line) and AAG (blue line)~~, respectively~~

To fix this problem, we tested various model settings and compiling options available in ROMS, such as increasing the number of vertical levels, changing the advection and diffusion schemes, horizontal mixing surfaces for tracers, and horizontal mixing schemes. The ~~D~~details of how the tested model settings effect on the spurious diapycnal mixing are beyond the scope of this paper, and they~~which~~ will be discussed in a separate paper.

The monthly mean temperature in theat 1000 m layer from for SCSOFSv2 varies from the initial conditions of 3.0 °C–-12.0 °C in initial condition to 3.0 °C–-11.5 °C (Fig.5d);, and the domain averaged monthly mean value increases slightly from the initial value of 4.4 °C in initial to 4.5 °C -(Fig.7a) in January inof the fifth model year (Fig.7a). The salinity at 1000 m varies from the 34.26-34.62 in initial conditions of 34.26–34.62 to 34.24–-34.63 (Fig. 6d);, and the domain averaged monthly mean value only slightly varies slightly from the initial value of 34.505 in initial to 34.509 (Fig.7b) in January inof the fifth model year (Fig. 7b). Theose values exhibitshow little variation untill January of the 11eleventh model year, the ranges are 3.0 °C–-11.3 °C for temperature (Fig. 5e) and 34.25–-34.63 for salinity (Fig. 6e), and the domain averaged values are 4.6 °C for temperature and 34.52 for salinity (Fig. 7), respectively. For tThe increment of the domain averaged value fors, temperature is about 0.2℃ and that for salinity is about 0.03, but theyyet remaining stable after 20 model years (Fig. 7). ThisIt is suggestssed that the spurious diapycnal mixing is significantlyhas been suppressed significantly by the AAG scheme combination, which can preserve the characteristics of the water masses in the deep ocean well. In additionMeantime, the temperature and salinity biases in the subsurface layer arehave been significantly improved significantly, which will be shown in the latter part of this paper.

In addition, it wais found that the model skill for the SST hais also significantly been improved significantly while using the new AAG scheme employed in SCSOFSv2 (Fig. 3 and Fig.4). The maximum of the monthly mean differences between the simulated SST simulated by SCSOFSv2 and OSTIA is about 3 °C–-4 °C, which is obviously smaller than the results of thefrom BulkFormula. Comparing with the results of SCSOFSv1 and BulkFormula, the results of SCSOFSv2 have a lowerless SST hot bias versus OSTIA is found in the central Pacific Ocean relative to OSTIA for the result of SCSOFSv2, which iscan be attributed to the new scheme combination scheme. TheFor the domain averaged RMSE of the monthly mean SST of SCSOFSv2 is about 0.65 °C–-0.84 °C, with an annual mean value of 0.77 °C., tThe maximum value (0.84 °C) is in January and December, and the minimum value (0.65 °C) is in May. Comparing with the results of the BulkFormula, the performance of the model skill based onjudging from the annual mean SST RMSE is improved by about 23% due to the usage of theemploying new combination scheme in SCSOFSv2. ItThis indicates that the subsurface or deep layer processes can affect the surface layer significantly due to vertical heat transport, which is induced by the barotropic and baroclinic instabilities that increas~~e~~ing~~ the eddy kinetic energy (Ding et al., 2021).

3.3 Data assimilation scheme

As was reported by~~mentioned as~~ Zhu et al. (2016), the original SCSOFSv1 used~~had employed~~ the multivariate Ensemble Optimal Interpolation (EnOI, Evensen, 2003; Oke et al., 2008) method to assimilate the along track altimeter Sea Level Anomaly (SLA) data produced by SSALTO/DUACS and distributed by AVISO with support from the Centre~~r~~ National D'études Spatiales. During this upgrading process, we also improved several of the ~~some~~ functions of the EnOI scheme~~,~~ and developed a new "Multi-source Ocean data Online Assimilation System" (MOOAS).

First~~ly~~, SCSOFSv1 only assimilated the along track SLA data~~ only~~, while SCSOFSv2 is also~~additionally~~ able to simultaneously assimilate satellite AVHRR SST and *in-situ* temperature and salinity vertical profile~~s~~ data from the Argo arrays~~, simultaneously~~. This~~It~~ is accomplished~~conducted~~ by combining~~constructing~~ the four variables'~~all~~ innovations (difference between the assimilated observation and the model forecast), background error covariances, and observation errors ~~for four different variables~~ into each~~one~~ array~~, respectively~~. It is worth to pointing out that~~,~~ the SLA data assimilated into the SCSOFS is a nearly real time along-track L3 product for special assimilation ~~specially~~, which is filtered but not subsampled and the~~with~~ ~~D~~dynamic a~~A~~tmospheric ~~C~~correction, ocean tide, long wavelength error correction is applied (CMEMS-SL-QUID-008-032-051, http://marine.copernicus.eu/documents/ QUID/CMEMS-SL-QUID-008-032-051.pdf). The filtering processing consists of~~in a~~ low-pass filtering with a cut-off wavelength of 65 km and a 20-day period using a Lanczos filter. The ~~R~~residual noise and small-~~-~~scale signals are then removed via~~by~~ filtering. For the measurement errors of the~~in~~ SCSOFSv2, we set those of the SLA as constants of 3 cm according to the method of Taburet et al. (2018)~~,~~ and directly used the estimated error standard deviation of the analysed AVHRR SST~~ directly, respectively;~~. ~~as f~~For those of the Argo profiles, assuming they are ~~represented as~~ a function of water depth (*D*) following Xie and Zhu (2010), ~~as~~ $ERR_T(D)=0.05+0.45\exp(-0.002D)$, and $ERR_S(D)=0.02+0.10\exp(-0.008D)$.

Second~~ly~~, we ~~have ~~introduced the method of computing the anomalies of the ensemble numbers used for constructing the background error covariance following Lellouche et al. (2013). In SCSOFSv1, the anomalies are computed by subtracting a 10-year average from ~~a ~~long-term (typically 10 years) model free run snapshots with a five~~5~~-day interval for the ocean state, i.e., the sea surface height and three-dimensional temperature, salinity, zonal velocity, and meridional velocity. In addition,~~And~~ the ensemble is selected within a 60-~~-~~day window around the target assimilation date from each year, resulting ~~adding~~ in a total of~~up to~~ about 130 members~~ in total~~ (Ji et al., 2015; Zhu et al., 2016). However, in SCSOFSv2, a Hanning low-pass filter is employed to create the running mean according to Lellouche et al. (2013) in order to obtain~~get~~ the intra-seasonal variability of~~in~~ the ocean state. Thus, the anomalies are computed by subtracting the running mean with a 20-day time window from the~~a~~ 10-year (2008-2017) free run daily averaged results. In particular~~Especially~~, it should be~~is~~ noted~~ pointed out~~ that the daily averaged free run results are selected within a 60~~-~~-day window, i.e.,~~with~~ 30 days before and after the target assimilation date from each year in~~of~~ 2008~~-~~–2017, and are used to compose the ensemble members, resulting in a total of~~thus totally~~ about 590 members in SCSOFSv2. This~~It~~ means that the background error covariances rely on a fixed basis and an intra-seasonally variable ensemble of anomalies, which improves the dynamic dependency.

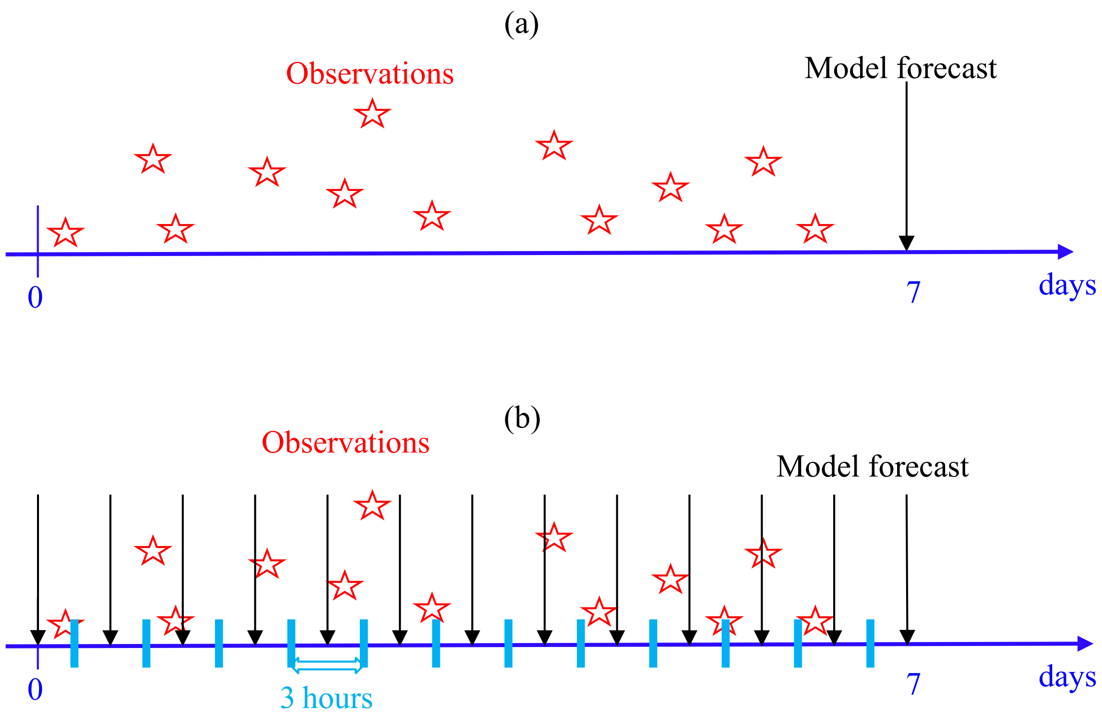

Figure 8: Schematic representation of the FGAT method: (a) not used in SCSOFSv1 ~~(a)~~ and (b) used in SCSOFSv2 ~~(b)~~. Red stars ~~stand for~~denote the observations, and the black arrows denote the~~stand for~~ archived snapshots of model forecast

Third~~ly~~, for each analysis step with a seven~~7~~-day assimilation cycle, all of the observations of the SLA within the seven~~7~~-day time window before the analysis time are treated as being observed at the analysis time in SCSOFSv1, with the assumption that~~of~~ all of the observations a~~we~~re still valid at the analysis time. The time misfit between the observation and the model forecast ~~would~~ causes non-negligible biases when calculating innovations. Actually, it is inconvenient to calculate all of the synchronous innovations between the observation and model forecast ~~entirely,~~ since the spatial~~o~~ and temporal distributions of the along-track SLA and Argo data are irregular and variable in~~at~~ each analysis step. In order to alleviate this deficiency, the First Guess at Appropriate Time (FGAT) method (Lee and Barker, 2005;Cummings, 2005;Lee et al., 2004;Sandery, 2018) wa~~i~~s used in SCSOFSv2. Considering the intense computing and storage costs, we ~~have~~ divided the ~~7~~seven-day time window into 56 three~~3~~-hour time slots (Fig. 8)~~,~~ and archived 57 snapshots with a three~~3~~-hour interval, while the model forecast was run following the previous analysis run. Then, the innovations were~~can be~~ calculated within each ~~3~~three-hour time slot ~~by~~

using the observations minus~~subtracts~~ the nearest model forecast. This~~It~~ means that the maximum temporal misfit of the innovations between the observation and the model forecast ~~would be~~were decreased from seven~~7~~ days to 1.5 hours by using FGAT. In addition~~Meanwhile~~, as in SCSOFSv1, the localization wa~~i~~s still used with the radius set to ~~be~~ 150 km~~ as in SCSOFSv1~~.

In SCSOFSv1, the analysis increments of the sea surface height and three-dimensional temperature, the salinity, and the zonal and meridional velocities produced by each analysis of the data assimilation we~~a~~re applied to the model's initial fields at one time step. This inevitably~~It would~~ induced a significant initial shock and spurious high-frequency oscillation in~~to~~ the model due to the imbalance between the increments and the model physics~~ inevitably~~ (Lellouche et al., 2013; Ourmières et al., 2006), and it usually resulted~~causes~~ in~~ a~~ rapid growth of the forecast error and even le~~a~~d to the model blowing-up after a few assimilation cycles or one or two~~-~~ years~~ period~~ after the intermittent assimilation run. This was~~It is~~ a threat to the stability and robustness of the OOFS. Therefore, we introduced the incremental analysis update (IAU) method (Bloom et al., 1996; Ourmières et al., 2006) to apply each analysis increment to the model integration as a forcing term in a gradual manner in SCSOFSv2 to diminish the negative impact. In this~~our~~ case, we obtained~~get~~ the tendency term by dividing the increments by~~with~~ the total number of time steps within an assimilation cycle, as in most IAU methodologies, in order to make sure the time integral of the tendency term equalled~~s~~ the analysis increment calculated by the EnOI.

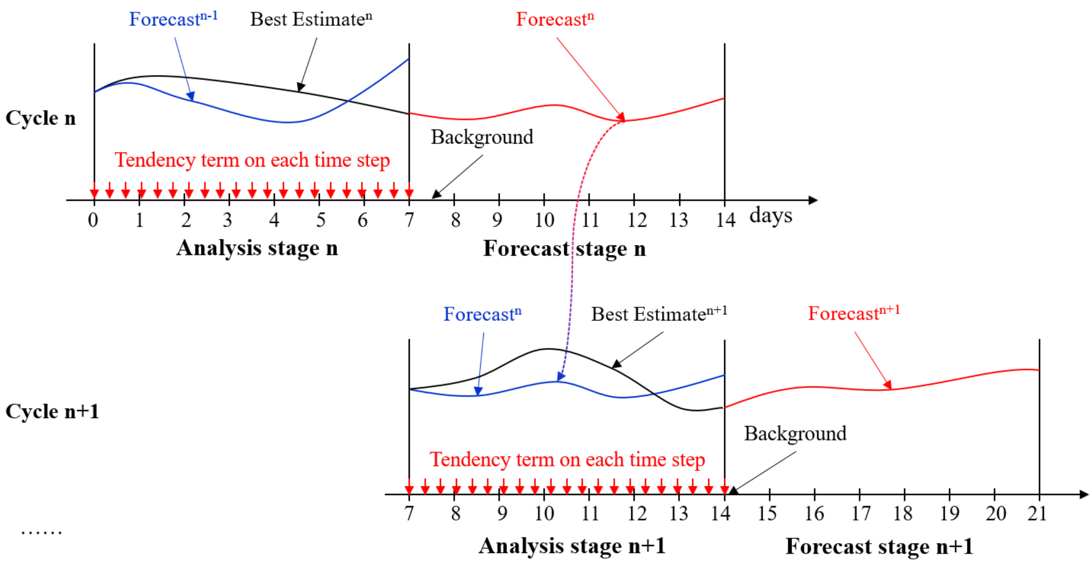

Figure 9: Schematic representation of the data assimilation procedure for two consecutive cycles, n and n+1, in SCSOFSv2, while considering the FGAT and IAU methods.

Once including the FGAT and IAU methods were included in the EnOI scheme, the entirewhole system's integral strategy hads to be adjusted by adding one more model integration over the assimilation time window (Lellouche et al., 2013). In SCSOFSv1, only one time model integration is needed only one time. ThisIt means that once physical ocean model finishes a seven7-day run (does not need to archive snapshot fields) and outputs a restart field., Tthe EnOI data assimilation module starts to calculate the analysis increments at the restart field time and adds it to the restart field,. tThen, the physical ocean model implementsmakes a hot-start from the updated restart field to run the seven7 days ofor the next cycle.

However, in SCSOFSv2, two times model integration areis needed twice due to the use ofconsidering the FGAT and IAU methods (Fig.8). ThisIt means that the physical ocean model needs to be integrated 14 days in each assimilation cycle, to add the tendency term to the model prognostic equations due to the IAU method used during the first seven-7 days run (referred to as the a"Analysis sStage"), to output a restart field at the end of 7th day for hot starting the ocean model in the next cycle, and to output 3three-hourly snapshots forecast fields during the second 7seven-days run (referred to as the "Fforecast sStage") to be used in the next cycle by the FGAT method. The model outputs from the Aanalysis sStage are referred to as the "Bbest Eestimate", and those from the Fforecast sStage are referred as "the Fforecast". The analysis increments are defined at the 3.5th day, but not at the end of the seven7th day as in SCSOFSv1., Twith the observed SLA and Argo vertical profiles data are within the seven7-day time window, and the AVHRR SST data on the 4fourth day are used by the FGAT method.

4. Inter-comparison and accuracy assessment

In order to demonstrateshow the improvements of the different SCSOFS sub-versions during the upgrading process, the results of the inter-comparison and assessment are presentedshown and discussed in this section, by using the GOV Inter-comparison and Validation Task Team (IV-TT) Class 4 verification framework (Hernandez et al., 2009). Class 4 metrics were originallyare used for inter-comparison and validation among different global or regional OOFSs or assimilation systems~~ originally~~ (Ryan et al., 2015; Hernandez et al., 2015; Divakaran et al., 2015). They~~It~~ include~~s~~ four metrics: the~~,~~ ~~namely,~~ bias for assessing the consistency, the RMSE for assessing the quality or accuracy, the anomaly correlation for assessing the pattern of the variability, and the skill scores for assessing the utility of a forecast. They are calculated according to differences between the model values and the reference measurements in observations space for each variable over a given period and spatial domain. The physical variables used in the Class 4 metrics are the SST, SLA, Argo profiles, surface currents, and sea ice. The r~~R~~eference measurements, providing the ocean "truth", are selected as follow:~~,~~ the SST data from the *in-situ* drifting BUOY, the SLA data from the AVISO along-track data, and the temperature and salinity data from the Argo profiles~~, respectively~~. They are assembled by GOV IV-TT participating partners on a daily basis (Ryan et al., 2015).

It is virtually impossible to exhaustively test and validate the ~~exhaustively~~ performances of all of the upgrades described~~mentioned~~ in Sections 2 and 3. Here, we separate the entire~~whole~~ upgrading procedure from SCSOFSv1 to SCSOFSv2 into four stages with three ~~more~~ sub-versions (v1.1, v1.2, and v1.3) according to the reality. ~~By respecting to the previous version,~~ T~~t~~he major upgrades to~~in~~ each new version with respect to the previous version are listed in Table 2.

Table 2 The major upgrades with respect to the previous version

SCSOFS versions	Settings updates
v1→v1.1	**ROMS version** changed~~shifting~~ from v3.5 to v3.7; **land-sea mask** redistribution; **bathymetry** substitution of ETOPO1 with GEBCO_2014; **initial temperature and salinity conditions** changed~~ing~~ from SODA2.2.4 to GDEMv3; **open boundary data** changed~~ing~~ from climatological monthly mean to monthly mean from 1990 to 2008 with SODA 2.2.4; **sea surface atmospheric forcing data** changed~~ing~~ from NCEP Reanalysis 2 to CFSR; **the parameter dQ/dSST** changed~~ing~~ from constant to temporally and spatially varying values; **sea surface atmospheric forcing method** changed~~ing~~ from direct~~ly~~ flux~~es~~ forcing to BulkFormula

v1.1→v1.2	**Open boundary data** of SODA 2.2.4 monthly mean extended~~ing~~ from 2008 to 2010; **the eastern lateral boundary** moved~~ing~~ westward; **the observed SST data** used for the net surface heat flux correction changed~~ing~~ from MGDSST to AVHRR
v1.2→v1.3	~~Considering~~ ~~m~~**Mean seal level atmospheric pressure** effect considered, ~~increasing~~ **vertical layers** increased from 36 to 50; ~~changing~~ **the transform and stretching function** changed; **tracers advection discrete schemes** changed~~ing~~ from UCI to AAG; ~~Changing the~~ **open boundary data** changed from SODA 2.2.4 monthly mean to SODA 3.3.1 and 3.3.2
v1.3→v2	~~Including t~~The MOOAS included

In this study~~paper~~, we used the Class 4 metric~~e~~s and selected the first four physical variables~~,~~ (SST, SLA, and Argo profiles)~~,~~ to inter-compare and assess the accuracies~~y~~ of the ~~among~~ different sub-versions of the SCSOFS (Table 3). Since none of~~all~~ the reference measurement~~s~~ data described~~mentioned~~ above have ~~not~~ been used in these sub-versions of SCSOFS ~~for those sub-versions~~ without data assimilation, they are ~~independent~~ reference observation independent from SCSOFS, except for SCSOFSv2. The inter-comparison and validation of the~~among those~~ sub-versions without data assimilation we~~a~~re conducted for the model free-run results in 2013, and the inter-comparison and validation between v1.3 and v2 we~~a~~re conducted in 2018 to validate the performance of the MOOAS.

Table 3 Mean values of each metric of the four physical variables for the best estimates of each sub-version (T denotes temperature, S denotes salinity, AC denotes anomaly correlation)

Variables	Metrics	v1	v1.1	v1.2	v1.3		v2
SST	AC	0.52	0.56	0.58	0.62	0.64	0.74
	Bias (°C)	0.77	0.88	0.70	0.40	0.34	0.24
	RMSE (°C)	1.21	1.12	0.98	0.76	0.66	0.52
SLA	AC	—	—	—	—	0.67	0.85
	Bias (cm)	−7.0	−5.5	−7.0	−7.4	−5.2	−3.1
	RMSE (cm)	21.6	20.8	16.7	14.8	12.9	8.5
T Profile	AC	0.01	0.04	−0.12	0.48	0.38	0.57
	Bias (°C)	0.98	0.75	0.30	−0.15	−0.08	0.15
	RMSE (°C)	1.75	1.60	1.44	1.03	0.96	0.67
S Profile	AC	−0.01	−0.02	0.02	0.44	0.30	0.51
	Bias	0.06	0.05	0.06	0.02	0.013	0.009
	RMSE	0.14	0.14	0.13	0.10	0.11	0.08
Year		2013				2018	

4.1 SST

The accuracy of the SST ~~is ~~continuously increased~~ing~~ from version v1 to v2, and the~~with~~ anomaly correlation increased from 0.52 in v1 to 0.74 in v2, i.e., a~~ with percentage increase being~~ 29.7% improvement.~~,~~ The RMSE ~~is ~~decreased~~ing~~ from 1.21℃ in v1 to 0.52℃ in v2, i.e., a~~with percentage increase being~~ 57.0% improvement, for the annual mean of the entire~~whole~~ model domain averaged in 2013 (or v1.3 and v2 in 2018) (Table 3). For ~~the ~~versions v1, v1.1, v1.2, and v1.3, their anomaly correlation exhibited~~shows~~ significant seasonal variations, with high anomaly correlations in summer and low anomaly correlations in winter. It wa~~i~~s also found~~indicated~~ that the accuracy of the SST~~ can be~~ benefited from the sea surface atmospheric forcing method, as well as the usage of more accurate observed SST data for the sea surface heat flux correction, temperature advection discrete scheme, and SST data assimilation.

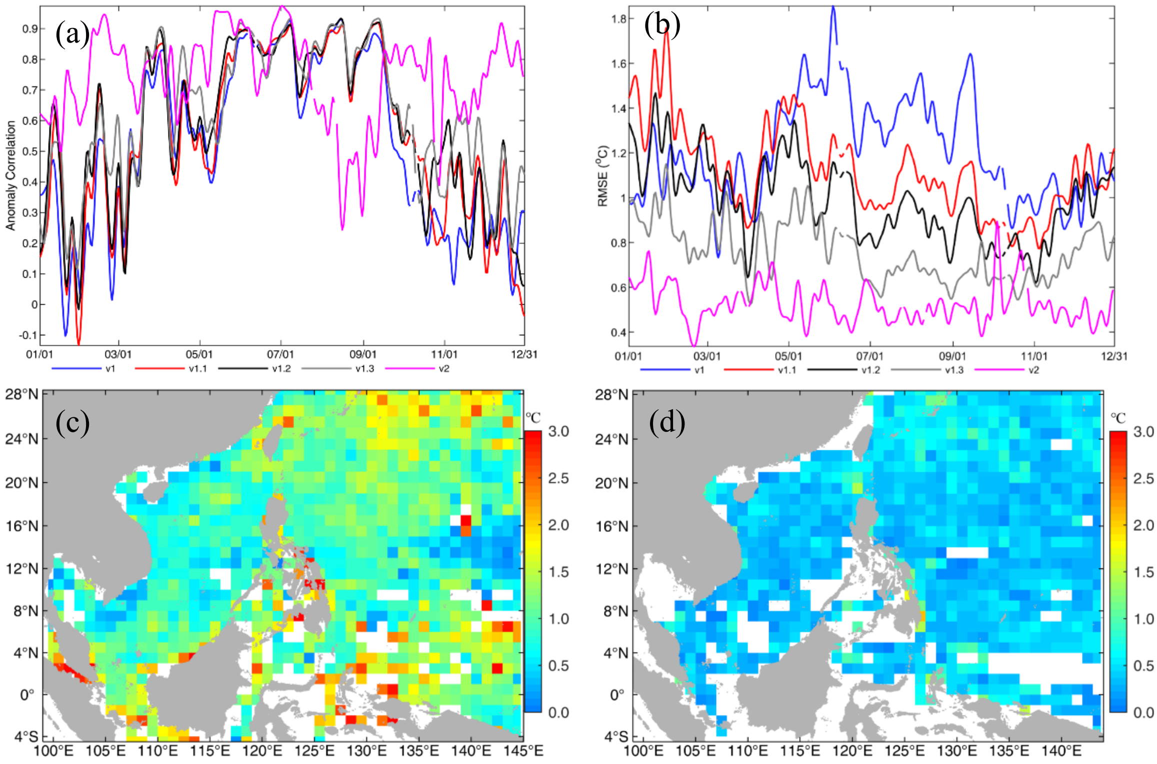

Figure 10: (a) Anomaly correlation ~~(a) ~~and (b) RMSE ~~(b) ~~time series of the SST best estimates for each version against observations as a function of time (seven~~7~~-day low~~-~~-pass filter applied), i.e., v1, v1.1, v1.2, and v1.3 without data assimilation in 2013~~,~~ and v2 with data assimilation in 2018. Horizontal distribution of the SST

RMSE in a 1°×1° bin for the versions (c) v1 (c) and (d) v2.(d), tThe calculations wereas performed for year-round in 2013 and 2018, respectively

The improvement of the SST due to sea surface atmospheric forcing method changeding mainly occurred in summer time, exhibitshowing the same pattern as the results ofor the year 2014 in Figs. 3 and 4. However, Butusing sea surface heat flux correction with more accurate observed SST data for the sea surface heat flux correctioncan improved accuracy of the SST simulation for the whole year-round (v1.2 in Fig. 10b). We also found that the OISST data wereis closer to the OSTIA than the MGDSST (figure not shown). Due to the benefits obtained from theose changes, the maximum and minimum values of the SST RMSE have decreased from 1.92 °C and 0.71 °C forin v1 to 1.52 °C and 0.60 °C forin v1.2 for the entirewhole year 2013, respectively. It is worth mentioning that the AAG schemes combination not only improveds the deep layer temperature, but it also contributeds to the improvement of the SST due to the internal baroclinic vertical heat transport. The maximum and minimum values of the SST RMSE wereis 1.21 °C and 0.52 °C forin v1.3. For the results with data assimilation in v2, the maximum and minimum values of the SST RMSE wereis only 1.13 °C and 0.32 °C, respectively,. whichIt are is better than the results forin v1.3 year-round.

For the horizontal distribution of the SST RMSE, the large values weare mainly located inat the areas near the equator, coastal areas, and the northern lateral boundary, with most of the values larger than 1.5 °C and a maximum value of about 6.67 °C forin v1 (Fig. 10c). ForIn v1.3, due to the contributions of all of the above described model updates, the pattern of the RMSE wais similar to that ofwith v1, i.e., basically without significant variations, but the maximum value decreaseds to 3.91 °C and most of the values weare less than 1.2 °C. After applying MOOAS in v2 (Fig. 10d), only a few large RMSE values weare located onat the eastern coast of Philippine Island, with athe maximum value of 2.09 °C, and most of the values were lower than 0.8 °C. ThisIt indicates that the performance of the SST in SCSOFSv2 whas been improved significantly improved by due to all of the updates describedmentioned above.

4.2 SLA

For the entire~~whole~~ upgrading process, the accuracy of the SLA~~ is~~ also continuously increased~~ing~~ from version v1 to v2, with the RMSE decreased~~ing~~ from 21.6 cm ~~in~~for v1 to 8.5 cm for~~in~~ v2, i.e.,~~ with percentage increase being~~ a 60.6% improvement, for the annual mean of the entire~~whole~~ model domain averaged in 2013 (or in 2018 for v1.3 and v2) (Table 3). Since there was an ongoing problem with the SLA climatology variable provided by GOV IV-TT during 2013–~~-~~2015, we could not calculate the anomaly correlation for the SLA in 2013 and had to provide feedbacked on this issue to GOV IV-TT. However, based on~~But from~~ the result of the SLA anomaly correlation in 2018, we ~~can ~~f~~i~~ound that it increased~~s~~ from 0.67 for~~in~~ v1.3 to 0.85 for~~in~~ v2, showing significant improvement in~~for~~ the correlation of the pattern of the variability between the model results and the climatology.

As can be seen f~~F~~rom Fig. 11(a), there wa~~i~~s a slight decrease in~~of~~ RMSE for~~in~~ v1.1 with respect to v1, which mainly occurs in winter ~~time, ~~and rarely in summer~~ time~~. This may be because there was no direct or intrinsic relationship between th~~os~~e model updates from v1 to v1.1 and the SLA in physics, and the~~o~~se updates mainly focused on the horizontal and temporal resolutions of the datasets. However, the improvement of the ~~SLA ~~accuracy of the SLA ~~is obvious ~~in v1.2 with respect to v1.1 was significant, with the minimum and maximum of daily-mean RMSE values decreasing~~change~~ from 0.12 cm and 0.31 cm for~~in~~ v1.1 to 0.11 cm and 0.23 cm for~~in~~ v1.2, respectively. Their annual mean value decreased~~s~~ from 20.8 cm for~~in~~ v1.1 to 16.7 cm ~~in~~for v1.2, i.e., ~~with percentage increase of ~~a 19.7% improvement. This may be the result~~ed~~ of the~~ from~~ well-~~-~~represented~~ing of~~ NEC pattern due to the change in the~~of~~ model's eastern lateral boundary. With respect to v1.2, the accuracy of the SLA in v1.3 increased slightly, ~~increases ~~with an annual mean value of 14.8 cm and a~~percentage increase~~ 11.4% improvement. This~~It~~ may be the result~~ed~~ of~~ from~~ the mean sea level air pressure correction and the modification of the temperature and salinity baroclinic structures due to the usage of the AAG~~ being employed~~. In addition, the most significant improvement in the~~for~~ SLA wa~~i~~s introduced by the MOOAS, with minimum and maximum ~~of ~~daily-mean RMSE values ~~ar~~of~~e~~ 6.1 cm and 12.1 cm for~~in~~ v2, respectively. The annual mean RMSE decreased~~s~~ to 8.5 cm and the percentage increase reached~~s to~~ 34.1% with respect to v1.3 and to 60.6% with respect to v1. This~~It ~~ significant improvement was ~~is ~~undoubtedly ~~that this significant~~

improvement is introduced bythe result of the along-track SLA being assimilated into the system by the MOOAS.

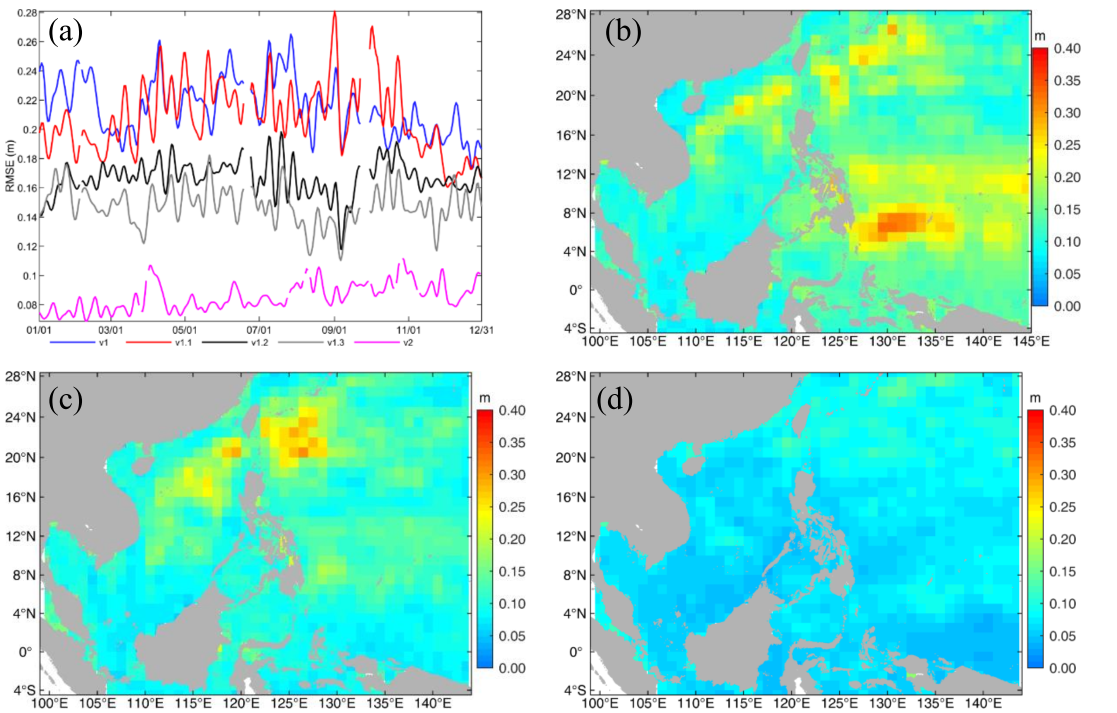

Figure 11: (a) similar to Fig. 10(b) but for the SLA. (b), (c), (d) similar to Fig.10 (c) or (d), but for the SLA ofin v1, v1.3 (in 2013), and v2, respectively.

For the horizontal distribution of the SLA RMSE, the large values of >over 20 cm weare mainly located in the area of the NEC pathway, the continental shelf of the northeastern SCS, and to the northeast of the Luzon Strait, with a maximum value of 32.7 cm forin v1 (Fig. 11b). ForIn v1.3 (Fig. 11c), the large values in the area of the NEC pathway almost disappeared, the maximum RMSE wais 30.3 cm and most of the values weare less than 20 cm, which canmay be interpreted as a better representationg of the NEC pattern due to amendment of the model's eastern lateral boundary. InBy comparisonng towith v1.3 or even v1, for v2, the SLA RMSE decreasedds dramatically for the entirewhole model domain and didoes not containshow areas with obvious large values in v2., and i Its maximum value wais only 18.2 cm, andwith most of the values were less than 10 cm. It is well known that abundantplenty mesoscale eddies occur oin botheach sides of the Luzon Strait, in the northeastern SCS, and in the western Pacific Ocean (Fig. 12a)., The large SLA RMSEs in Figs. 11b and Fig. 11c indicateing that a pure physical ocean model cannot capture these meso-scale processes well without assimilating SLA data ~~assimilated~~ (Fig.12b). However, Fig. 11d shows a significant reduction in the~~with~~ SLA RMSE, indicating that the meso-scale eddies can be represented by SCSOFSv2 due to assimilation of the ~~with~~ along-track SLA data, ~~assimilated~~ and the results are in good agreement with the satellite observations ~~well~~ (Fig. 12c).

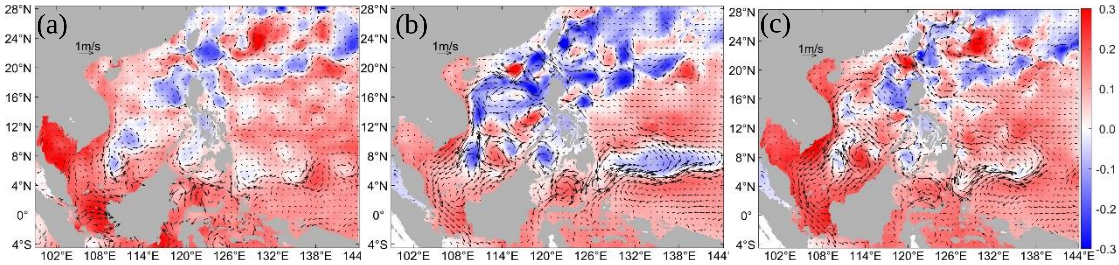

Figure 12: Daily averaged SLA (colour shading~~ed~~) and surface velocity anomaly (vectors) on January 15, 2018, from AVISO, SCSOFSv1.3, and SCSOFSv2~~, respectively~~.

4.3 Temperature and salinity profiles

For the three-dimensional temperature and salinity distribution, by comparing the model results with the climatology temperature and salinity profiles, the results of ~~from~~ first three versions exhibit~~show~~ poor correlations with the observations (Figs. 13a and ~~Fig.~~14a) and have large RMSEs (Figs. 13b and ~~Fig.~~14b), i.e., 1.44 °C–1.75 °C for temperature and 0.13–0.14 for salinity (Table 3), even though~~if~~ they decrease due to the~~with~~ model updates. In particular~~Especially~~, for the vertical distribution, the RMSE can reach ~~to larger than~~ 3°C for temperature and 0.3 for salinity in the thermocline and halocline, respectively, and it remains~~ed~~ larger than 1 °C for temperature in the deep layer and 0.1 for salinity above a depth of 700 m ~~depth~~ (Figs. 13d and ~~Fig.~~14d). This may result from the spurious diapycnal mixing caused by the~~due to~~ UCI ~~schemes~~ combination scheme~~employed~~. Th~~os~~e updates to~~in~~ v1.1 and v1.2 can only slightly improved the three-dimensional temperature and salinity, and they did ~~can~~not contribute to their intrinsic improvements for~~,~~ neither ~~for~~ surface forcing nor ~~for~~the lateral boundary conditions, with the~~an~~ exception of the surface layer with depths of less~~shallower~~ than 100 m.

However, once the AAG ~~schemes~~ combination scheme was implemented ~~employed~~ in v1.3, the improvements to the three-dimensional temperature and salinity we~~a~~re significant~~obvious~~ with respect to the first three versions (Figs. 13a,b and ~~Fig.~~14a,b). The anomaly correlation increase~~d~~s to 0.38–0.48 for temperature and 0.30–0.44 for salinity, and the RMSE decrease~~d~~s to 0.96 °C–1.03 °C~~°C~~ for temperature and 0.10–0.11 for salinity, respectively (Table 3). For the vertical distribution, the anomaly correlation remaineds at around 0.4 for both temperature and salinity in the entirewhole water column, and it was greater than over 0.6 for temperature in the surface layer (Figs.13c and Fig.14c)., The RMSEs significantly decreased to less than 2 °C for temperature in the thermocline, and 0.25 for salinity in the halocline, and less than 1°C for temperature and 0.1 for salinity in the deep layer (Figs.13d and Fig.14d). For the horizontal distribution of the three-dimensional temperature and salinity RMSEs, the RMSE of the temperature iwas more likely to being more than ≥1.5 °C with maximum and minimum values ofbeing 4.45 °C and 0.49 °C (Fig. 13e), respectively; whike theand RMSE of salinity wasis greatlarger than 0.1, with

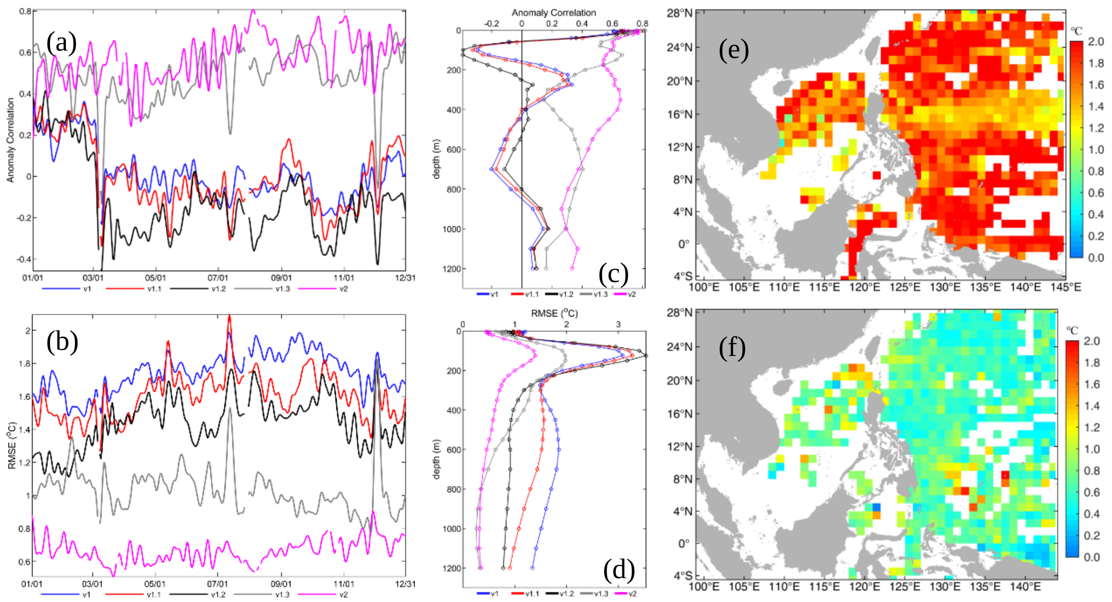

Figure 13: (a) and (b) similar to Figs.10(a) and (b) but for the temperature profile, respectively. (c) and (d)) vertical distributions of best estimates for each sub-version against observations as a function of depth, v1, v1.1, v1.2, and v1.3 without data assimilation in 2013, and v2 with data assimilation in 2018. (e) and (f) similar to Figs. 10(c) and (d), but for the temperature profile in v1 and v2, respectively.

maximum and minimum values ofbeing 0.81 and 0.06 (Fig.14e), respectively, for in v1. The lLarge values for salinity were mainly located in the SCS and near the equator in the Pacific Ocean. The trend waıs the same as thewith time series of the RMSE., tThe horizontal distributions of the temperature and salinity RMSEs shows slight decreased slightly from version v1 to v1.2, but they dramatically decreased in v1.3 (Ffigures not shown). Since it is benefited from the usage of the AAG schemes combination scheme in v1.3, most of the temperature RMSEs were~~is~~ lower than 1.0 °C, with maximum and minimum values of~~being~~ 1.72 °C and 0.11 °C, respectively; and most of the salinity RMSEs were~~is~~ less than 0.1, with maximum and minimum values of~~being~~ 0.62 and 0.03 in 2013, respectively.

By employing the MOOAS, the accurac~~y~~ies of the three-dimensional temperature and salinity were~~has been improved~~ continuously improved in v2 compared to v1.3 for all of the metrics in 2018 (Figs. 13 and ~~Fig.~~14). The mean anomaly correlations ~~has~~ increased from 0.38 to 0.57 for temperature~~,~~ and from 0.30 to 0.51 for salinity. The mean RMSEs ~~has~~ decreased from 0.96 °C to 0.67 °C for temperature, and from 0.11 to 0.08 for salinity (Table 3). For the vertical distributions of the anomaly correlation for temperature, it wa~~'~~s ~~over~~ >0.6 in the surface layer, was~~over~~ >0.4 above 600 m, and was~~over~~ >0.3 in the deep layer (Fig. 13c). The RMSE of the temperature wa~~i~~s less than 1.5 °C for the entire~~whole~~ vertical profile, and similar to in other versions, the maximum value ~~i~~was located in~~at~~ the thermocline ~~similar with other versions~~, but the error decreased~~s~~ dramatically (Fig. 13d). In contrast to~~Unlike~~ temperature, the vertical anomaly correlation of the salinity did~~oes~~ not ~~show~~ significantly improve below 200 m ~~ment~~ in v2 with respect to v1.3 ~~below 200m~~, and it was only~~shows a little~~ slightly higher than that of~~which in~~ v1.3 (Fig. 14c) ~~in~~ above 200 m. The~~S~~ salinity RMSE ~~i~~was less than 0.25 for the entire~~whole~~ vertical profile, with the maximum value located at the surface and decreasing with depth~~,~~ and decreasing~~e~~ to less than 0.05 below 600 m (Fig. 14d).

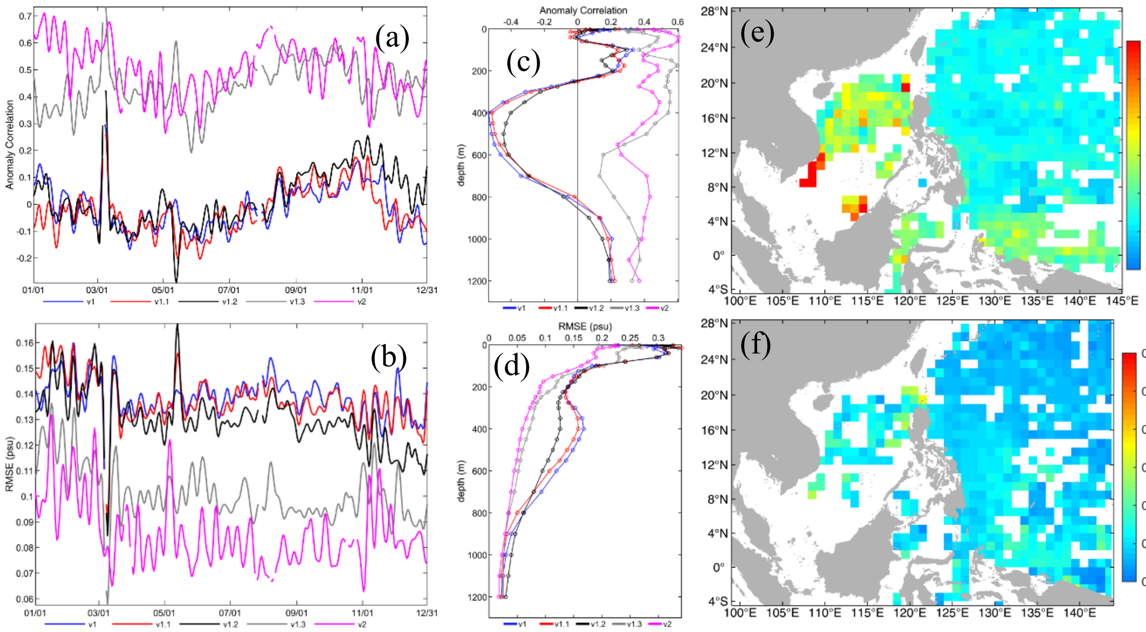

Figure 14: Similar to Fig. 13, but for salinity profile.

For the horizontal RMSE distribution ofin v2, most of the temperature RMSEs wereis greatlarger than 0.8 °C with maximum and minimum values ofbeing 1.96 °C and 0.03 °C (Fig. 13f), respectively; and most of the salinity RMSEs wereis greater than 0.1, with maximum and minimum values ofbeing 0.35 and 0.01 (Fig.14f), respectively, in 2018 (Fig. 14f).

5. Conclusions

The results of Tthis study illustrate thes major updates applied made to SCSOFSv1 in termsaspects of the physical model settings, inputs, and EnOI data assimilation scheme in the last fewrecent couple years following the recommendations of Zhu et al. (2016), such as redistributions of the land-water grid mask redistribution,; changes in the data sources ofor the bathymetry, the initial conditions, and the sea surface forcing method; changing the and open boundary conditions changing to higher spatial and temporal resolutions;, shifting the eastern lateral boundary westward;, and increasing the vertical layers of the model, and so on.

The Tthree most significant updates weare highlighted in this paper. Firstly, the sea surface atmospheric forcing method hwas been changed from direct forcing to the BulkFormula to acquire an effective negative feedback mechanism ofor the air–-sea interactions by using the COARE3.0 bulk algorithm. The Uupgrades lead to more reasonable SST simulations withby eliminating of abnormal values, significantly decreasdropping of the maximum value of the monthly mean differences between the simulated SST and OSTIA, and decreasing theof domain averaged RMSE of the monthly mean SST from 0.99 °C–-1.62 °C in SCSOFSv1 to 0.87 °C–-1.15 °C in the BulkFormula run. The annual mean value decreaseds from 1.27 °C to 1.00 °C, indicating that the performance of model's skill has improved by about 21%.

Secondly, the AAG scheme was substituted for the tracers advection term discrete scheme UCI has been substituted with AAG in order to suppress the spurious diapycnal mixing problem. After this substitution, the domain averaged monthly mean temperature in theat 1000 m layer decreaseds from 5.1 °C to 4.5 °C, and thatwhich of the salinity decreaseds from 34.54 to 34.509, in January of the fifth model year, respectively. Even after 20 model years, the domain averaged values of the temperature and salinity increments we~~a~~re only about 0.2 °C and 0.03, respectively, suggesting that the AAG combination scheme~~s combination~~ can well~~ preserve~~ the characteristics of the water masses in the deep ocean preserve. In addition, the model skill for the SST also ~~can~~ benefited from the AAG combination scheme,~~s~~ and the~~combination with~~ annual mean domain averaged RMSE decreased~~ing~~ from 1.00 °C to 0.77 °C, i.e., ~~showing~~a 23% improvement~~ing~~ in~~rate for~~ the performance.

Third~~ly~~, the original EnOI method in SCSOFSv1 ~~h~~was~~ been~~ upgraded to the~~new~~ MOOAS by adding four new functions. The multi-source observation data (SST, SLA, and Argo profiles) were~~can be~~ simultaneously assimilated.~~ simultaneously;~~ The Hanning high-pass filter wa~~i~~s applied to the ensemble members from 10 years of free run while calculating the background error covariances to improve the dynamic dependency.~~;~~ The FGAT method with a ~~3~~three-hour time slot wa~~i~~s used to calculate the innovations; and the IAU technique with a~~is employed with 7~~seven-day time window was used to ~~apply~~ analyse~~is~~ the increment in~~to~~ the model integration in a gradual manner.

Moreover, inter-comparison and accuracy assessment of the~~among~~ five versions we~~a~~re conducted based on the GOV IV-TT Class 4 metrics for four physical variables, i.e., the SST, SLA, and Argo profiles. The improvement in the~~of~~ accuracy of the simulated SST was mainly due~~attributes~~ to the use of more accurate observed SST data ~~source used~~ for the sea surface heat flux correction, the use of the BulkFormula method for the sea surface atmospheric forcing, and the use of the AAG discrete temperature advection~~ discrete~~ scheme. The improvement of the~~SLA~~ accuracy of the SLA as mainly due to the~~benefits from~~ good representations of the NEC pattern obtained~~caused~~ by modify~~icat~~i~~o~~ng ~~of~~the model's eastern lateral boundary, the mean sea level air pressure correction, and the improvement of the three-dimensional temperature and salinity baroclinic structures ~~improvement due to~~by using the AAG scheme~~employed~~. The improvement of the three-dimensional temperature and salinity mainly benefited~~s~~ from the use of the AAG non-spurious diapycnal mixing combination scheme~~s combination employed~~.

Finally~~At last~~, the remarkable improvements in~~for~~ all of the above four variables ~~are~~ also benefited from use of the MOOAS~~ application~~. With respect to v1.3, for the v2 using the MOOAS, the domain averaged annual mean SST RMSE decreased~~s~~ from 0.66 °C to 0.52 °C, i.e., a~~with percentage increase being~~ 21.2% improvement.~~,~~ The SLA RMSE decreased~~s~~ from 12.9 cm to 8.5 cm, i.e., a~~ with percentage increase being~~

34.1% improvement.~~,~~ The temperature profile's RMSE decrease~~ds~~d from 0.96 ℃ to 0.67 ℃, i.e., a~~with percentage increase being~~ 30.2% improvement.~~,~~ The salinity profile's RMSE decrease~~ds~~d from 0.11 to 0.08, i.e., a ~~with percentage increase being~~ 27.3% improvement~~, in v2 while using MOOAS~~.

Although SCSOFSv2 is greatly~~has~~ improved ~~greatly~~ compar~~ing~~ed to the previous versions, some biases still exist, such as the structures of the temperature and salinity profiles in the subsurface, especially in~~for~~ the thermocline and halocline. We plan to continue to improve the system in terms of both the physical model settings and the data assimilation scheme in the~~for~~ next step, including a~~such as~~ sub-grid parameterization scheme for the unresolved physical processes, a vertical turbulent mixing scheme to consider wave mixing, a more accurate input and forcing data source, and assimilati~~ng~~on of more or new types of observations (glider or mooring three-dimensional temperature and salinity profiles, drifting buoys, *in-situ* velocity data from moorings) into the system.

Code and Data availability. The latest version of the source code for EnOI and ROMS trunk used to producethe results in this paper can be accessed via https://doi.org/10.5281/zenodo.5215783. GEBCO_2014 Grid, https://www.bodc.ac.uk/data/open_download/gebco/GEBCO_30_SEC/zip/, last access 3 January 2021; SODA 3.3.1, https://www2.atmos.umd.edu/~ocean/index_files/soda3.3.1_mn_download.htm, last access 3 January 2021; SODA3.3.2, https://dsrs.atmos.umd.edu/DATA/soda3.3.2/REGRIDED/ocean/, last access 3 January 2021; CFSR, http://rda.ucar.edu/datasets/ds093.0, last access 3 January 2021; CFSv2, http://rda.ucar.edu/datasets/ds094.0, last access 3 January 2021; NCEP_Reanalysis 2, https://www.psl.noaa.gov/data/gridded/data.ncep.reanalysis2.html, last access 3 January 2021; AVHRR, http://www.ncei.noaa.gov/data/sea-surface-temperature-optimum-interpolation/v2.1/access/avhrr/, last access 3 January 2021; OSTIA, SST of *in-situ* drifting BUOY, AVISO along-track SLA, and Argo temperature and salinity profiles, https://marine.copernicus.eu/, last access 3 January 2021.

Author Contributions. XZ performed the physical model improvement and free-run simulations, designed and wrote the paper. XZ and ZZ updated MOOAS and performed the data assimilation simulations. SR and AL analysed and assessed model results. SR, HW and YZ helped in reading and commenting on the paper. MZ helped in polishing the paper.

Competing interests. The authors declare that they have no conflict of interest.

Acknowledgements. This work was supported by the project of Southern Marine Science and

Engineering Guangdong Laboratory (Zhuhai) (No. SML2020SP008, 311020004), the National Natural Science Foundation of China (NO. 42176029， 41806003). We would like to thank the anonymous reviewers for their careful reading of the manuscript and for providing constructive comments to improve the manuscript.

References

Bao, X., Wan, X., Gao, G., and Wu, D.: The characteristics of the seasonal variability of the sea surface temperature field in the Bohai Sea, the Huanghai Sea and the East China Sea from AVHRR data, Acta Oceanol. Sin., 24, 125-133, 2002.

Barnier, B., Siefridt, L., and Marchesiello, P.: Thermal forcing for a global ocean circulation model using a three-year climatology of ECMWF analyses, J. Mar. Syst., 6, 363-380, 10.1016/0924-7963(94)00034-9, 1995.

Barnier, B., Patrick, M., Miranda, A. P. D., Molines, J.-M., and Coulibaly, M.: A sigma-coordinate primitive equation model for studying the circulation in the South Atlantic. Part I: Model configuration with error estimates, Deep Sea Res. (I Oceanogr. Res. Pap.), 45, 543-572, 1998.

Bloom, S. C., Takacs, L. L., Silva, A. M. D., and Ledvina, D.: Data Assimilation using incremental Analysis Updates, Monthly Weather Review, 124, 1256-1271, 1996.

Beckmann, A., Haidvogel, D.B.: Numerical simulation of flow around a tall isolated seamount. Part I: problem formulation and model accuracy. J. Phys. Oceanogr. 23, 1737-1753, 1993.

Cai, S., Xie, J., Xu, J., Wang, D., Chen, Z., Deng, X., and Long, X.: Monthly variation of some parameters about internal solitary waves in the South China sea, Deep Sea Res. Pt I, 84, 73-85, 10.1016/j.dsr.2013.10.008, 2014.

Carnes, M. R.: Description and Evaluation of GDEM-V3.0, Stennis Space Center, MS, 2009.

Carton, J. A., and Giese, B. S.: A Reanalysis of Ocean Climate Using Simple Ocean Data Assimilation (SODA), Monthly Weather Review, 136, 2999-3017, 10.1175/2007MWR1978.1, 2008.

Carton, J. A., Chepurin, G. A., and Chen, L.: SODA3: A New Ocean Climate Reanalysis, J. Clim., 31, 6967-6983, 10.1175/JCLI-D-18-0149.1, 2018.

Chu, P. C., and Li, R.: South China Sea isopycnal-surface circulation, J. Phys. Oceanogr., 30, 2419-2438, 10.1175/1520-0485(2000)030, 2000.

Cummings, J. A.: Operational multivariate ocean data assimilation, Quart. J. R. Met. Soc., 131, 10.1256/qj.05.105, 2005.

Ding, R., Xuan, J., Zhang, T., Zhou, L., Zhou, F., Meng, Q., Kang, I.: Eddy-Induced Heat Transport in the South China Sea, J. Phys. Oceanogr., 51(7): 2329-2349, 10.1175/JPO-D-20-0206.1, 2021.s

Divakaran, P., Brassington, G. B., Ryan, A. G., Regnier, C., Spindler, T., Mehra, A., Hernandez, F., Smith, G. C., Liu, Y., and Davidson, F.: GODAE OceanView Inter-comparison for the Australian Region, Journal of Operational Oceanography, 8, s112-s126, 10.1080/1755876X.2015.1022333, 2015.

Dombrowsky, E., Bertino, L., Brassington, G. B., Chassignet, E. P., Davidson, F., Hurlburt, H. E., Kamachi, M., Lee, T., Martin, M. J., Mei, S., and Tonani, M.: GODAE systems in operation, Oceanography, 22, 80-95, 10.5670/oceanog.2009.68, 2009.

Donlon, C. J., Martin, M., Stark, J., Roberts-Jones, J., Fiedler, E., and Wimmer, W.: The Operational Sea Surface Temperature and Sea Ice Analysis (OSTIA) system, Remote Sens. Environ., 116, 140-158, 10.1016/j.rse.2010.10.017, 2012.

Evensen, G.: The Ensemble Kalman Filter: Theoretical formulation and practical implementation, Ocean Dynam., 53, 343-367, 10.1007/s10236-003-0036-9, 2003.

Fairall, C. W., Bradley, E. F., Hare, J. E., Grachev, A. A., and Edson, J. B.: Bulk Parameterization of Air–Sea Fluxes: Updates and Verification for the COARE Algorithm, J. Clim., 16, 571-591, 2003.

Farris, A., and Wimbush, M.: Wind-induced Kuroshio intrusion into the South China Sea, J. Oceanogr., 52, 771-784, 10.1007/BF02239465, 1996.

Hellerman, S., and Rosenstein, M.: Normal Monthly Wind Stress Over the World Ocean with Error Estimates, J. Phys. Oceanogr., 13, 1093-1104, 1983.

Hernandez, F., Bertino, L., Brassington, G. B., Chassignet, E., Cummings, J., Davidson, F., Drevillon, M., Garric, G., Kamachi, M., Lellouche, J.-M., Mahdon, R., Martin, M. J., Ratsimandresy, A., and Regnier, C.: Validation and intercomparison studies within GODAE, Oceanography, 22, 128-143, 10.5670/oceanog.2009.71, 2009.

Hernandez, F., Blockley, E., Brassington, G. B., Davidson, F., Divakaran, P., Drévillon, M., Ishizaki, S., Garcia-Sotillo, M., Hogan, P. J., Lagemaa, P., Levier, B., Martin, M., Mehra, A., Mooers, C., Ferry, N., Ryan, A., Regnier, C., Sellar, A., Smith, G. C., Sofianos, S., Spindler, T., Volpe, G., Wilkin, J., Zaron, E. D., and Zhang, A.: Recent progress in performance evaluations and near real-time assessment of operational ocean products, J. Operat. Oceanogr., 8, s221-s238, 10.1080/1755876X.2015.1050282, 2015.

Hwang, C., and Chen, S.-A.: Circulations and eddies over the South China Sea derived from TOPEX/Poseidon altimetry, J. Geophys. Res., 105, 23943-23965, 10.1029/2000JC900092, 2000.

Ji, Q., Zhu, X., Wang, H., Liu, G., Gao, S., Ji, X., and Xu, Q.: Assimilating operational SST and sea ice analysis data into an operational circulation model for the coastal seas of China. Acta Oceanol. Sin., 34, 54-64, 10.1007/s13131-015-0691-y, 2015.

Kanamitsu, M., Ebisuzaki, W., Woollen, J., Yang, S.-K., Hnilo, J. J., Fiorino, M., and Potter, G. L.: Ncep-Doe Amip-II reanalysis (R-2), Bull. Amer. Meteor. Soc., 83, 1631-1643, 10.1175/BAMS-83-11-1631, 2002.

Kourafalou, V. H., Mey, P. D., Hénaff, M. L., Charria, G., Edwards, C. A., He, R., Herzfeld, M., Pascual, A., Stanev, E. V., Tintoré, J., Usui, N., Westhuysen, A. J. v. d., Wilkin, J., and Zhu, X.: Coastal Ocean Forecasting: system integration and evaluation, J. Oper. Oceanogr., 8, s127-s146, 10.1080/1755876X.2015.1022336, 2015.

Large, W. G., and Yeager, S. G.: The global climatology of an interannually varying air–sea flux data set, Clim. Dynam., 33, 341-364, 10.1007/s00382-008-0441-3, 2009.

Lee, M.-S., Barker, D., Huang, W., and Kuo, Y.-H.: First Guess at Appropriate Time (FGAT) with WRF 3DVAR, Preprints for WRF/MM5 Users' Workshop, Boulder, CO, 22-25 June 2004.

Lee, M.-S., and Barker, D.: Preliminary Tests of First Guess at Appropriate Time (FGAT) with WRF 3DVAR and WRF Model, Asia-Pac. J. Atmos. Sci., 41, 495-505, 2005.

Lellouche, J.-M., Galloudec, O. L., Drevillon, M., Regnier, C., Greiner, E., Garric, G., Ferry, N., Desportes, C., Testut, C.-E., Bricaud, C., Bourdalle-Badie, R., Tranchant, B., Benkiran, M., Drillet, Y., Daudin, A., and Nicola, C. D.: Evaluation of global monitoring and forecasting systems at Mercator Ocean, Ocean Sci., 9, 57-81, 10.5194/os-9-57-2013, 2013.

Lellouche, J.-M., Greiner, E., Galloudec, O. L., Garric, G., Regnier, C., Drevillon, M., Benkiran, M., Testut, C.-E., Bourdalle-Badie, R., Gasparin, F., Hernandez, O., Levier, B., Drillet, Y., Remy, E., and Traon, P.-Y. L.: Recent updates to the Copernicus Marine Service global ocean monitoring and forecasting real-time 1/12° high-resolution system, Ocean Sci., 14, 1093-1126, 10.5194/os-14-1093-2018, 2018.

Li, A.，Zhang, M.，Zhu, X., Zu, Z., Wang, H.: A research on the optimal approach of CFSR surface flux data correction based on different surface forcing modes. Haiyang Xuebao，2019, 41(11)：51–63，doi:10.3969/j.issn.0253−4193.2019.11.006 (In Chinese with English abstract)

Li, A., Zhu, X., Zhang, Y., Ren, S., Zhang, M., Zu, Z., Wang, H.: Recent improvements to the physical model of the Bohai Sea, the Yellow Sea and the East China Sea Operational Oceanography Forecasting System, Acta Oceanologica Sinica, 2021, 40(9): 1-17, doi: 10.1007/s13131-021-1840-0.

Li, B., Cao, A., and Lv, X.: Three-dimensional numerical simulation of M2 internal tides in the Luzon Strait, Acta Oceanol. Sin., 34, 10.1007/s13131-015-0748-y, 2015.

Li, H., Song, D., Chen, X., Qian, H., Mu, L., and Song, J.: Numerical study of M2 internal tide generation and propagation in the Luzon Strait, Acta Oceanol. Sin., 30, 23-32, 10.1007/s13131-011-0144-1, 2011.

Liu, Z., Chen, X., Yu, J., Xu, D., and Sun, C.: Kuroshio intrusion into the South China Sea with an anticyclonic eddy: evidence from underwater glider observation, J. Oceanol. Limnol., 37, 1469-1480, 10.1007/s00343-019-8290-y, 2019.

Mao, Q., Shi, P., and Qi, Y.: Sea surface dynamic topography and geostrophic current over the South China Sea from Geosat altimeter observation, Acta Oceanol. Sin., 21, 11-16, 1999.

Marchesiello, P., Debreu, L., and Couvelard, X.: Spurious diapycnal mixing in terrain-following coordinate models: The problem and a solution, Ocean Model., 26, 156-169, 10.1016/j.ocemod.2008.09.004, 2009.

Nan, F., Xue, H., and Yu, F.: Kuroshio intrusion into the South China Sea: A review, Prog. Oceanogr., 137, 314-333, 10.1016/j.pocean.2014.05.012, 2015.

Naughten, K. A., Galton-Fenzi, B. K., Meissner, K. J., England, M. H., Brassington, G. B., Colberg, F., Hattermann, T., and Debernard, J. B.: Spurious sea ice formation caused by oscillatory ocean tracer advection schemes, Ocean Model., 116, 108-117, 10.1016/j.ocemod.2017.06.010, 2017.

Oke, P. R., Brassington, G. B., Griffin, D. A., and Schiller, A.: The Bluelink ocean data assimilation system (BODAS), Ocean Model., 21, 46-70, 10.1016/j.ocemod.2007.11.002, 2008.

Ourmières, Y., BRANKART, J.-M., BERLINE, L., BRASSEUR, P., and VERRON, J.: Incremental Analysis Update Implementation into a Sequential Ocean Data Assimilation System, J. Atmos. Ocean. Technol., 23, 1729-1744, 2006.

Qiu, B., and Chen, S.: Interannual-to-Decadal Variability in the Bifurcation of the North Equatorial Current off the Philippines, J. Phys. Oceanogr., 40, 2525-2538, 10.1175/2010JPO4462.1, 2010.

Ryan, A. G., Regnier, C., Divakaran, P., Spindler, T., Mehra, A., Smith, G. C., Davidson, F., Hernandez, F., Maksymczuk, J., and Liu, Y.: GODAE OceanView Class 4 forecast verification framework: global ocean inter-comparison, J. Oper. Oceanogr., 8, s98-s111, 10.1080/1755876X.20151022330, 2015.

Saha, S., Moorthi, S., Pan, H. L., Wu, X., Wang, J., Nadiga, S., Tripp, P., Kistler, R., Woollen, J., Behringer, D., Liu, H., Stokes, D., Grumbine, R., Gayno, G., Wang, J., Hou, Y. T., Chuang, H. Y., Juang, H. M. H., Sela, J., Iredell, M., Treadon, R., Kleist, D., Van Delst, P., Keyser, D., Derber, J., Ek, M., Meng, J., Wei, H., Yang, R., Lord, S., Van Den Dool, H., Kumar, A., Wang, W., Long, C., Chelliah, M., Xue, Y., Huang, B., Schemm, J. K., Ebisuzaki, W., Lin, R., Xie, P., Chen, M., Zhou, S., Higgins, W., Zou, C. Z., Liu, Q., Chen, Y., Han, Y., Cucurull, L., Reynolds, R. W., Rutledge, G., and Goldberg, M.: The NCEP climate forecast system reanalysis, Bull. Amer. Meteor. Soc., 91, 1015-1057, 10.1175/2010BAMS3001.1, 2010.

Saha, S., Moorthi, S., Wu, X., WANG, J., NADIGA, S., TRIPP, P., BEHRINGER, D., HOU, Y.-T., CHUANG, H.-Y., IREDELL, M., EK, M., MENG, J., YANG, R., MENDEZ, M. P., DOOL, H. V. D., ZHANG, Q., WANG, W., CHEN, M., and BECKER, E.: The NCEP Climate Forecast System Version 2, J. Clim., 27, 10.1175/JCLI-D-12-00823.1, 2014.

Sandery, P.: Data assimilation cycle length and observation impact in mesoscale ocean forecasting, Geosicentific Model Development, 11, 4011-4019, 10.5194/gmd-11-4011-2018, 2018.

Shchepetkin, A. F., and McWilliams, J. C.: A method for computing horizontal pressure-gradient force in an oceanic model with a nonaligned vertical coordinate, J. Geophys. Res., 108, 3090, 10.1029/2001JC001047, 2003.

Shchepetkin, A. F., and McWilliams, J. C.: The regional oceanic modeling system (ROMS): a split-explicit, free-surface, topography-following-coordinate oceanic model, Ocean Model., 9, 347-404, 10.1016/j.ocemod.2004.08.002, 2005.

Song, Y., and Haidvogel, D.: A Semi-implicit Ocean Circulation Model Using a Generalized Topography-Following Coordinate System, J. Comp. Phys., 115, 228-244, 10.1006/jcph.1994.1189, 1994.

Taburet, G., SL-TAC team. Quality Information Document for Sea Level TAC DUACS Products, Copernicus Marine Environment Monitoring Service, 2.4, 2018.

Tonani, M., Balmaseda, M., Bertino, L., Blockley, E., Brassington, G. B., Davidson, F., Drillet, Y., Hogan, P., Kuragano, T., Lee, T., Mehra, A., Paranathara, F., Tanajura, C. A. S., and Wang, H.: Status and future of global and regional ocean prediction systems, J. Oper. Oceanogr., 8, s201-s220, 10.1080/1755876X.2015.1049892, 2015.

Tsujino, H., Usui, N., and Nakano, H.: Dynamics of Kuroshio path variations in a high-resolution general circulation model, J. Geophys. Res., 111, C11001, 10.1029/2005JC003118, 2006.

Usui, N., Ishizaki, S., Fujii, Y., Tsujino, H., Yasuda, T., and Kamachi, M.: Meteorological Research Institute multivariate ocean variational estimation (MOVE) system: Some early results, Adv. Space Res., 37, 806-822, 10.1016/j.asr.2005.09.022, 2006.

Usui, N., Wakamatsu, T., Tanaka, Y., Hirose, N., Toyoda, T., Nishikawa, S., Fujii, Y., Takatsuki, Y., Igarashi, H., Nishikawa, H., Ishikawa, Y., Kuragano, T., and Kamachi, M.: Four-dimensional variational ocean reanalysis: a 30-year high-resolution dataset in the western North Pacific (FORA-WNP30), J. Oceanogr., 73, 205-233, 10.1007/s10872-016-0398-5, 2017.

Wang, J.: Global Linear Stability of the Two-Dimensional Shallow-Water Equations: An Application of the Distributive Theorem of Roots for Polynomials on the Unit Circle, Mon. Weather Rev., 124, 1301-1310, 1996.

Wang, Q., Zeng, L., Chen, J., He, Y., Zhou, W., and Wang, D.: The Linkage of Kuroshio Intrusion and Mesoscale Eddy Variability in the Northern South China Sea: Subsurface Speed Maximum, Geophys. Res. Lett., 47, 10.1029/2020GL087034, 2020.

Wang, W., Wang, D., Zhou, W., Liu, Q., Yu, Y., and Li, C.: Impact of the South China Sea Throughflow on the Pacific Low-Latitude Western Boundary Current: A Numerical Study for Seasonal and Interannual Time Scales, Adv. Atmos. Sci., 28, 1367-1376, 10.1007/s00376-011-0142-4, 2011.

Wei, Z., Li, S., Susanto, R. D., Wang, Y., Fan, B., Xu, T., Sulistiyo, B., Adi, T. R., Setiawan, A., Kuswardani, A., and Fang, G.: An overview of 10-year observation of the South China Sea branch of the Pacific to Indian Ocean throughflow at the Karimata Strait, Acta Oceanol. Sin., 38, 1-11, 10.1007/s13131-019-1410-x, 2019.

Xie, J., Zhu, J.: Ensemble optimal interpolation schemes for assimilating Argo profiles into a hybrid coordinate ocean model, Ocean Modelling, 33(3–4): 283–298, 10.1016/j.ocemod.2010.03.002.

Xu, D., Zhuang, W., and Yan, Y.: Could the two anticyclonic eddies during winter 2003/2004 be reproduced and predicted in the northern South China Sea?, Ocean Sci., 15, 97-111, 10.5194/os-15-97-2019, 2019.

Zhang, S., Qiu, F., Zhang, J., Shen, J., and Cha, J.: Monthly variation on the propagation and evolution of internal solitary waves in the northern South China Sea, Cont. Shelf Res., 171, 21-29, 10.1016/j.csr.2018.10.014, 2018.

Zhang, Z., Tian, J., Qiu, B., Zhao, W., Chang, P., Wu, D., and Wan, X.: Observed 3D Structure, Generation, and Dissipation of Oceanic Mesoscale Eddies in the South China Sea, Sci. Rep., 6, 24349, 10.1038/srep24349, 2016.

Zhao, Z., and Alford, M. H.: Source and propagation of internal solitary waves in the northeastern South China Sea, J. Geophys. Res., 111, 1-14, 10.1029/2006JC003644, 2006.

Zheng, Q., Xie, L., Zheng, Z., and Hu, J.: Progress in Research of Mesoscale Eddies in the South China Sea, Adv. Mar. Sci., 35, 131-158, 10.3969/j.issn.1671-6647.2017.02.001, 2017.

Zhu, X., Wang, H., Liu, G., Régnier, C., Kuang, X., DakuiWang, Ren, S., Jing, Z., and Drévillon, M.: Comparison and validation of global and regional ocean forecasting systems for the South China Sea, Nat. Hazards Earth Syst. Sci., 16, 1639-1655, 10.5194/nhess-16-1639-2016, 2016.

Zu, Y., Sun, S., Zhao, W., Li, P., Liu, B., and Fang, Y.: Seasonal characteristics and formation mechanism of the thermohaline structure of mesoscale eddy in the South China Sea, Acta Oceanol. Sin., 38, 29-38, 10.1007/s13131-018-1222-4, 2019.